Geochemistry Geophysics Geosystems G3
AN ELECTRONIC JOURNAL OF THE EARTH SCIENCES
Published by AGU and the Geochemical Society

Technical Brief
Volume 6, Number 9
27 September 2005
Q09P02, doi:10.1029/2005GC000930
ISSN: 1525-2027

Identification and removal of Mn-Mg-rich contaminant phases on foraminiferal tests: Implications for Mg/Ca past temperature reconstructions

L. D. Pena
GRC Geociències Marines, Department of Stratigraphy, Paleontology and Marine Geosciences, University of Barcelona, C/ Martí i Franquès, s/n, E-08028 Barcelona, Spain (lpena@ub.edu)

E. Calvo
Research School of Earth Sciences, Australian National University, Canberra, ACT 0200, Australia

Now at Centre Mediterrani d'Investigacions Marines i Ambientals, CMIMA-CSIC, Passeig Marítim de la Barceloneta, 37-49, E-08003 Barcelona, Spain

I. Cacho
GRC Geociències Marines, Department of Stratigraphy, Paleontology and Marine Geosciences, University of Barcelona, C/ Martí i Franquès, s/n, E-08028 Barcelona, Spain

Godwin Laboratory, Department of Earth Sciences, University of Cambridge, Pembroke Street, Cambridge CB2 3SA, UK

S. Eggins
Research School of Earth Sciences, Australian National University, Canberra, ACT 0200, Australia

C. Pelejero
Research School of Earth Sciences, Australian National University, Canberra, ACT 0200, Australia

Now at Centre Mediterrani d'Investigacions Marines i Ambientals, CMIMA-CSIC, Passeig Marítim de la Barceloneta, 37-49, E-08003 Barcelona, Spain

[1] The geochemical composition of foraminifera shells from an Ocean Drilling Program site in the Panama Basin has been analyzed by several analytical techniques (LA-ICP-MS, ICP-MS, XRD, SEM, EDX) in order to identify and evaluate the occurrence of contaminant phases which may bias paleoenvironmental reconstructions. LA-ICP-MS results on uncleaned tests indicate the presence of Mn-Mg-rich contaminant phases at the inner surfaces of the foraminiferal shells (which have Mn/Ca ratios up to 400 mmol mol^{-1} and Mg/Ca ratios up to 50 mmol mol^{-1}). We have rigorously assessed the ability of different cleaning protocols to remove these contaminant phases and have obtained satisfactory results only when a reductive step is included. The analysis of cleaning residuals collected after each of the different cleaning steps applied reveals that high Mn values are associated with at least two different contaminant phases, of which only one is linked to high Mg values. XRD analysis further reveals that the Mn-Mg-rich phase is the Ca-Mn-Mg carbonate kutnahorite ($Ca(Mn, Mg)(CO_3)_2$). Our results demonstrate that the presence of kutnahorite-like minerals can bias Mg/Ca ratios toward higher values (by 7–36%) and lead to significant overestimation of past seawater temperatures (by 0.9 up to 6.2°C, in the case of these Panama Basin samples).

Components: 11,867 words, 13 figures, 3 tables.

Keywords: calcium carbonate; foraminifera; kutnahorite; laser ablation; Mg/Ca; Ocean Drilling Program.

Index Terms: 4825 Oceanography: Biological and Chemical: Geochemistry; 4954 Paleoceanography: Sea surface temperature; 4994 Paleoceanography: Instruments and techniques.

Received 1 February 2005; **Revised** 5 July 2005; **Accepted** 21 July 2005; **Published** 27 September 2005.

Pena, L. D., E. Calvo, I. Cacho, S. Eggins, and C. Pelejero (2005), Identification and removal of Mn-Mg-rich contaminant phases on foraminiferal tests: Implications for Mg/Ca past temperature reconstructions, *Geochem. Geophys. Geosyst.*, *6*, Q09P02, doi:10.1029/2005GC000930.

Theme: Developmentof the Foraminiferal Mg/Ca Proxy for Paleoceanography
Guest Editor: Pamela Martin

1. Introduction

[2] During the last decades, many paleoceanographic studies have used foraminiferal elemental composition as a proxy for seawater paleoenvironmental conditions [e.g., *Cronblad and Malmgren*, 1981; *Delaney et al.*, 1985; *Boyle*, 1988]. In particular, the foraminiferal Mg/Ca ratio is now being widely used as a seawater paleotemperature proxy [*Nürnberg et al.*, 1996; *Rosenthal et al.*, 1997a; *Hastings et al.*, 1998; *Lea et al.*, 1999; *Elderfield and Ganssen*, 2000]. Nevertheless, Mg/Ca seawater thermometry is still under development with factors that can bias shell Mg/Ca composition and lead to inaccurate reconstructions of past-oceanographic environments remaining poorly constrained. Several processes that may significantly alter the original Mg/Ca ratio of foraminiferal calcite include the postmortem addition of diagenetic phases [*Boyle*, 1981, 1983], selective dissolution of the carbonate tests [e.g., *Dekens et al.*, 2002], and the presence of silicates or other contaminant phases [*Barker et al.*, 2003]. In particular, the presence of Mn-rich carbonate overgrowths (and Mn-rich oxyhydroxides) are known to be a serious problem for trace element analyses of foraminifera, because manganese carbonate may contain high levels of other trace elements and significantly alter the ''natural'' composition of foraminifera carbonates [*Boyle*, 1983]. However, the extent to which these manganese enrichments bias Mg/Ca temperature reconstructions has not been rigorously evaluated, with the identification of contaminant phases and a full assessment of the effectiveness of different cleaning protocols yet to be performed. The latter is significant because foraminifera cleaning protocols have progressively evolved from the methods developed initially by *Boyle* [1981], *Boyle and Keigwin* [1985] and *Lea and Boyle* [1991], adding or removing steps in the cleaning process depending on the particular requirements of the samples being analyzed.

[3] Currently used cleaning methodologies can be divided into two main groups: ''Oxidative'' cleaning protocols and ''Reductive'' cleaning protocols. ''Oxidative'' cleaning protocol (also referred as ''Mg cleaning'' protocol) comprise a number of clay removal steps, an (oxidizing) organic matter elimination step and a final weak acid leaching [*Elderfield and Ganssen*, 2000; *Barker et al.*, 2003]. ''Reductive'' cleaning protocol (also referred as ''Cd cleaning'' protocol) includes an additional reductive step, either prior to or after the oxidative step, which is designed to eliminate any Mn-Fe-oxyhydroxides present on the foraminifera shells [*Boyle and Keigwin*, 1985; *Lea and Boyle*, 1991; *Rosenthal et al.*, 1999; *Martin and Lea*, 2002]. Although originally the reductive step was set up after the oxidative step, these were latter exchanged to allow the removal of insoluble sulfide mineral phases like cadmium sulfide (CdS) [*Rosenthal et al.*, 1995; *Boyle and Rosenthal*, 1996; *Rosenthal et al.*, 1997b]. The use of these cleaning strategies by different laboratories has implications for the comparison and reliability of determined Mg/Ca seawater temperature estimates as inconsistencies between different cleaning methodologies are known to produce significant differences in measured Mg/Ca compositions [*Rosenthal et al.*, 2004].

[4] The advent of microanalytical techniques such as secondary ion mass spectrometry (SIMS), and the electron microprobe, and more recently laser ablation inductively coupled plasma mass spectrometry (LA-ICP-MS), have greatly improved our ability to scrutinize and understand the distribution of trace elements within and on the surfaces of foraminifera shells. The relatively new application of LA-ICP-MS to characterize the composition of planktonic [*Eggins et al.*, 2003, 2004; *Hathorne*

et al., 2003; S. Eggins et al., manuscript in preparation, 2005] and benthic [*Wu and Hillaire-Marcel*, 1995; *Reichart et al.*, 2003] foraminifera, has already been demonstrated to have considerable potential in paleoceanographic studies, as well as ecology through the reconstruction of habitat migrations [*Eggins et al.*, 2003, 2004]. The possible applications of LA-ICP-MS in the field of paleoceanography remain only partly explored and in the present work, we extend the use of LA-ICP-MS to the identification and characterization of contaminant phases present in foraminifera shells.

[5] In this study, a complement of analytical techniques (ICP-MS, DRX and SEM-EDX) has been employed in conjunction with LA-ICP-MS to analyze and characterize foraminiferal samples from the Panama basin, a Mn-enriched basin. Moreover, different cleaning protocols are monitored to evaluate their effectiveness in removing Mn-Mg-rich contaminant phases. We are able to characterize a Mn-Mg-rich phase and evaluate its influence in paleotemperature reconstructions on the basis of Mg/Ca ratios in these samples.

2. Manganese Geochemistry in the Panama Basin

[6] The studied samples are from the Panama Basin ODP Site 1240, Leg 202 (0° 01.31'N, 86° 27.76'W and 2921 m of water depth; Figure 1). Primary production in the region is controlled by the dynamics of the equatorial upwelling driven by southeasterly trade winds. The level of biological productivity in the region is among the highest found in the oceans [*Moore et al.*, 1973]. Oceanographic conditions that favor upwelling together with a tectonic setting that promotes hydrothermal production causes the delivery of relatively large amounts of both biogenic reactive organic carbon and hydrothermal manganese, respectively, to the sea floor [*Aller*, 1990, and references therein]. An additional source of dissolved manganese comes through a relatively unaltered seawater flow in the underlying basement which has been well constrained in regions of the central equatorial Pacific [*Baker et al.*, 1991]. The large supply of organic carbon to the bottom raises the consumption of oxygen, and results in oxygen depletion within a few centimeters of the sediment-water interface [*Pedersen and Price*, 1982; *Reimers*, 1987; *Johnson et al.*, 1996]. This promotes manganese reduction reactions that are capable of oxidizing the entire estimated annual flux of carbon [*Aller*, 1990]. Dissolution of buried manganese oxides in deeper

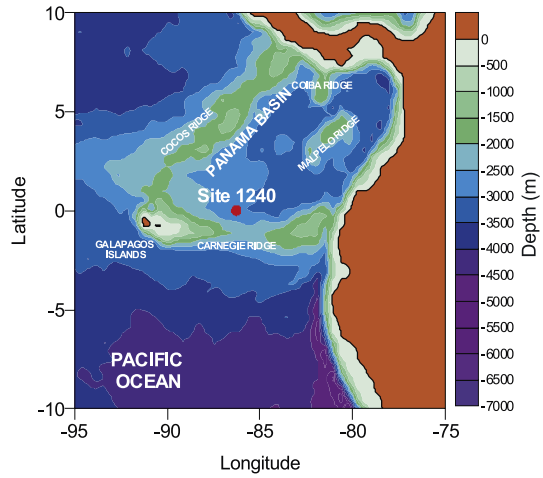

Figure 1. Map showing the area of study and ODP Site 1240 at the Panama Basin. Color scale highlighting major bathymetric features [*British Oceanographic Data Centre*, 2003].

sediments sections which display reducing conditions can result in an upward diffusion of dissolved Mn(II) ions and reprecipitation of Mn(IV) as oxides where higher redox potentials prevail, usually near the sediment-water interface [*Pedersen and Price*, 1982]. Some of the dissolved Mn(II) is accumulated in the oxic surface layer and, together with hydrothermal manganese, generates regional surface enrichments in the sediments. Under anoxic conditions the maximum dissolved manganese concentration in the interstitial pore waters is typically limited by the precipitation of manganese carbonates. Authigenic Mn-carbonate phases have been previously identified in sediments from the Panama Basin [*Pedersen and Price*, 1982; *Boyle*, 1983]. Such carbonates phases are impure, consisting of varying proportions of manganese, calcium, magnesium and often iron.

3. Methodology

3.1. Laser Ablation ICP-MS

[7] A high-resolution, LA-ICP-MS compositional depth profiling technique, developed at the Australian National University and described in detail by *Eggins et al.* [2003, 2004], has been employed to measure variation in Mg/Ca, Mn/Ca and Sr/Ca ratios through the walls of both whole and fragmented shells. The laser ablation system comprises a pulsed ArF Excimer laser ($\lambda = 193$ nm), linked to an Agilent 7500s quadrupole mass spectrometer via a custom built laser ablation cell and sample transport system. A moderately low laser fluence

(4 J/cm2) was used to shave a 30 μm diameter and uniformly (~0.1 μm) thick layer from the targeted surface of the shell wall with each laser pulse which, together with an ablation cell design that minimizes particulate residence times ($t^1/_2 \sim 0.35$ s), provides submicron depth resolution. A relatively small number of isotopes and trace elements were simultaneously measured by repeated, rapid sequential peak hopping (1 point/peak, dwell time = 10–30 ms) between selected isotopes (including ^{24}Mg, ^{25}Mg, ^{43}Ca, ^{44}Ca, ^{55}Mn), while laser ablation sampling proceeds through the shell wall. Material ablated from progressively deepening ablation pits was transported via a mixed Ar-He gas flow to the ICP-MS, which was optimized for sensitivity across the analyte mass range and also low molecular species production (by maintaining ThO^+/Th^+ <0.5%). Data reduction from raw time-resolved spectra, includes screening of spectra for outliers, subtraction of mean background intensities (measured with the laser off), and calibration of instrument response using the NIST610 glass standard reference material.

3.2. Solution ICP-MS

[8] All solution ICP-MS measurements were carried out at the analytical services unit of the University of Barcelona using a Perkin Elmer Elan6000, quadrupole ICP-MS. Mass resolution was 0.7 amu (atomic mass units). The instrument was tuned for maximum sensitivity and stability. The sample introduction system consisted of a micro-autosampler (PE-AS91) device attached to a "cross-flow" nebulizer with flow rates of 0.7 l min^{-1} and 1 ml min^{-1} for the nebulizer gas (Argon) and sample gas, respectively. Multiple isotopes were simultaneously analyzed (^{43}Ca, ^{44}Ca, ^{24}Mg, ^{26}Mg, ^{88}Sr, ^{55}Mn, ^{27}Al, ^{114}Cd and ^{111}Cd) by rapid sequential peak hoping, using Rh^{103} as the internal standard. Most elements were measured using the detector in analogue mode to avoid detector saturation and matrix effects [*Lea and Martin*, 1996], except ^{114}Cd and ^{111}Cd that were measured in pulse counting mode because of their relatively low concentration. Dwell times for the majority of measured isotopes were set to 100 ms except ^{44}Ca and ^{43}Ca, which were set to 20 and 50 ms, respectively. Each element measurement consisted of 20 readings with corresponding integration times amounting to 2000 ms, with the exception of ^{44}Ca and ^{43}Ca for which total integration times were 400 and 1000 ms, respectively. Four replicate measurements per sample were performed to improve analytical precision.

[9] Standard solutions were prepared from primary standards (High Purity Standards, 1000 ± 3 μg mL^{-1} in 1% Aristar grade HNO_3) and mixed to produce as multi-element stock solution. Four working standards were prepared by successive dilutions of the stock standard solutions to match the Ca concentrations typically found in the samples (10, 20, 50 and 100 ppm). Working standards were measured and corrected for background noise by means of blank sample subtraction. Elemental concentrations were recalibrated every 15 analyses.

3.3. X-Ray Diffraction

[10] X-Ray Diffraction (XRD) analyses were performed on about 20 mg of foraminiferal calcite with an INEL CPS-120 diffractometer at the analytical services unit of the University of Barcelona. Due to the expected low proportion of the contaminant phase compared to foraminiferal calcite in our samples, the X-ray diffractometer was set for long integration times (12 hours), in order to obtain a very high resolution X-ray diffractogram. The resulting diffraction patterns were processed using PCPDFWIN v. 2.2 software, and mineral phase identification accomplished by comparison with the International Center for Diffraction Data (ICDD®) database.

3.4. SEM-EDX

[11] Scanning Electron Microscopy (SEM) images were obtained using Jeol JSM-840 and Cambridge Instruments SEMs, at the analytical services of the University of Barcelona and a S360, Cambridge Instruments SEM at the Electron Microscope Unit of the Australian National University. Energy Dispersive X-ray (EDX) microanalyses of the selected samples (Table 1) were performed using the Jeol JSM-840 system in Barcelona. Foraminifera shell fragments were selected from those remaining after each cleaning protocol step and placed on carbon tape prior to carbon coating for EDX elemental microanalysis (at U. Barcelona) and gold coating for SEM imaging (at ANU).

3.5. Cleaning Procedures

[12] The cleaning protocols of foraminifera shells performed in this study are based on the original works by *Boyle* [1981] and *Boyle and Keigwin* [1985], adopting some of the modifications suggested by *Barker et al.* [2003]. Their main steps are described below. In our experiment, we performed both the "oxidative" cleaning protocol and the "reductive" cleaning protocol, following essentially

Table 1. Samples Selected for Analyses and Original ICP-MS Mn/Ca Values[a]

Sample ID[b]	ODP Sample Code Leg/Site/Hole/Core/Sect/ Interval, cm	Depth, mcd[c]	Species	Mn/Ca, mmol/mol	Mg/Ca, mmol/mol
SR-1	ODP 202/1240/B/1H/1/37–39	0.37	*G. ruber*	2.25	3.08
SR-2	ODP 202/1240/B/1H/2/140–142	2.91	*G. ruber*	1.51	2.66
SR-3	ODP 202/1240/B/1H/4/100–102	5.52	*G. ruber*	1.02	2.34
SR-5	ODP 202/1240/B/2H/2/144–146	14.71	*G. ruber*	5.97	4.38
SD-1	ODP 202/1240/B/1H/1/37–39	0.37	*N. dutertrei*	0.29	0.99
SD-2	ODP 202/1240/B/1H/2/140–142	2.91	*N. dutertrei*	0.41	0.98
SD-3	ODP 202/1240/B/1H/4/100–102	5.52	*N. dutertrei*	0.28	0.95
SD-4	ODP 202/1240/B/2H/2/144–146	13.5	*N. dutertrei*	2.03	1.54
SD-5	ODP 202/1240/C/2H/2/116–118	14.71	*N. dutertrei*	5.49	2.36

[a] Oxidatively cleaned samples.
[b] Sample label.
[c] Meters composite depth.

the same steps. The "reductive" cleaning protocol includes all the steps described below from A to E whereas the "oxidative" cleaning protocol includes all steps but C. Blank samples were routinely performed within every batch of samples in order to monitor potential contamination from reagents and vials.

3.5.1. Foraminifera Crushing and Clay Removal

[13] Foraminifera individuals were picked from a specific size fraction (315–355 μm), with care being taken to select the best preserved and apparently cleanest tests. These were then crushed between two clean glass plates under the microscope in order to allow chamber fills and contaminant phases to escape during the cleaning. After transferring the sample to suitable, acid leached, 0.5 ml Eppendorf vials, three ultra-pure MilliQ water rinses were performed in order to bring clays into suspension. Special care was taken to remove the residuals while clays were still in suspension. Afterward, two methanol rinses were carried out for further clay removal due to the lower methanol viscosity that allows attached clays to escape into solution. Finally, one more MilliQ water rinse was performed to eliminate any methanol residue.

3.5.2. Oxidative Cleaning

[14] The foraminifera walls very often preserve remains of organic matter, usually accompanied by high levels of magnesium [*Hastings et al.*, 1996; *Rathburn and De Deckker*, 1997]. An oxidative step is thus necessary to avoid potential biases to Mg/Ca foraminifera analyses. We used an alkali buffered (NaOH) hydrogen peroxide (H_2O_2) 1% solution that reacted with the sample in a boiling water bath for 10 minutes. After 5 minutes, samples were briefly sonicated to promote reaction and to facilitate the contact of the reagent with the sample since the presence of gas bubbles can prevent contact between the solution and the sample. After oxidation, samples were rinsed three times with MilliQ water to eliminate H_2O_2 remains and prevent any further reaction.

3.5.3. Reductive Cleaning

[15] This step aims removing a variety of contaminants phases such as Mn oxides that can commonly be found associated to foraminifera tests. As a reductive reagent, we used a mixture of hydrazine hydroxide, citric acid and ammonia hydroxide (caution must be taken when using this combination of reagents due to its extremely high toxicity and explodes on contact with oxidants). 100 μl of the reductive mixture was added to each vial, securing caps to prevent the sample from popping open upon reaction. The sample rack was placed inside a hot (about 100°C) ultrasonic bath during 30 minutes and sonicated briefly every 2 minutes to promote the reaction. After this step the reagent was removed from the vial and the sample was washed 3 times with ultra pure MilliQ water. Then, two more rinses with hot (about 80°C) MilliQ water, waiting for 5 minutes in each rinse, were performed, followed by a final rinse with cold MilliQ water. A proper removal of any reagent residue is very important at this stage to avoid reaction with chemicals used in the following steps and further dissolution of the samples.

3.5.4. Weak Acid Leaching

[16] The main objective of this step is to eliminate any remaining contaminant phase or particle that could be still attached to the foraminifera walls. 250 μl of diluted HNO_3 (0.001M) were added to

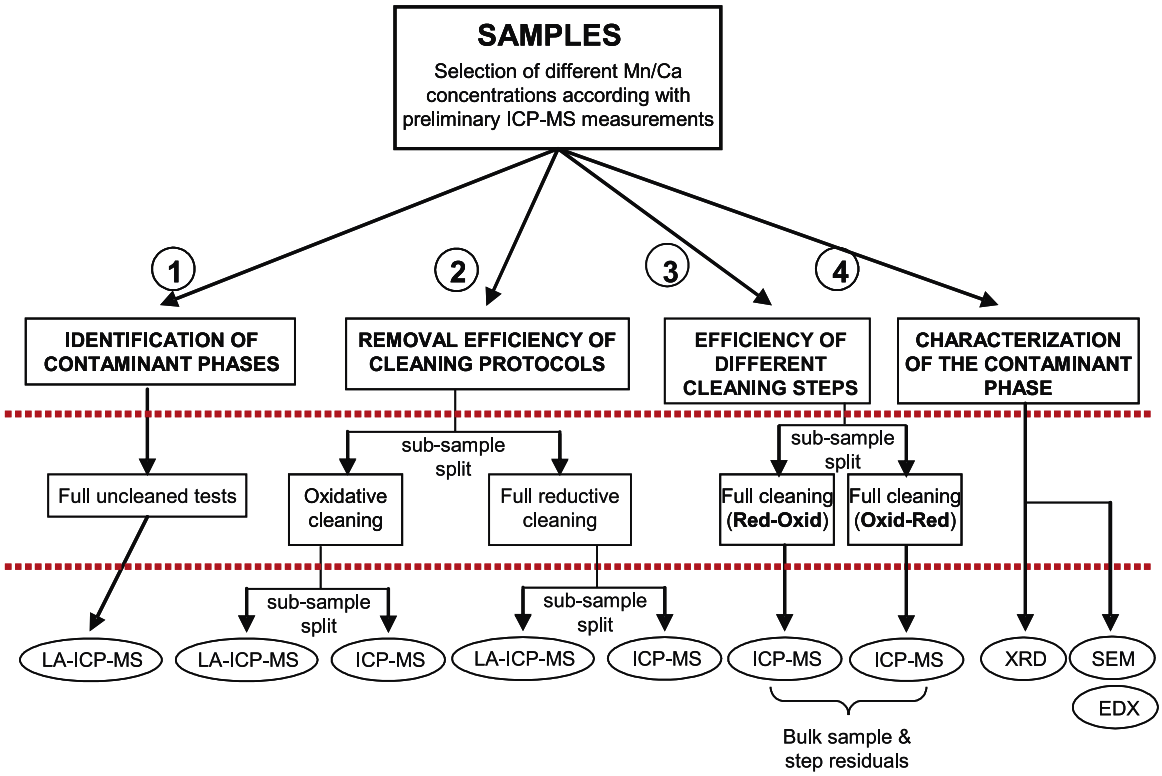

Figure 2. Schematic view of the experimental design developed during this study. Note the differences between expected objectives, samples manipulation, and the analytical method employed on each part of this work.

the sample and sonicated during 30s. After this leaching, the supernatant solution was removed and the samples were rinsed three times with MilliQ water to prevent extensive dissolution of the sample.

3.5.5. Final Dissolution, Centrifugation, and Transfer to Clean Vials

[17] In this last step, the samples were dissolved in ultra-pure HNO_3 (1%) and centrifuged during 5 minutes (6000 rpm). Then, the solution was transferred to clean vials (ready to be analyzed by ICP-MS) leaving a small residue of solution in the old vial to avoid any left solid impurity.

3.6. Experimental Design

[18] For the purposes of this study, we designed an experiment that was structured in four different phases (Figure 2): (1) detection of contaminant phases attached to the foraminifera walls (LA-ICP-MS), (2) evaluation of the efficacy of the two main cleaning protocols (“oxidative” and “reductive” protocols) to remove Mn-Mg-rich contaminants (LA-ICP-MS and ICP-MS), (3) assessment of the effectiveness of every single cleaning step to remove a suite of elements (solution-ICP-MS), and (4) characterization and identification of the Mn-Mg-rich mineral phase (XRD, SEM and EDX).

[19] Analyses were performed mainly in samples of *Neogloboquadrina dutertrei* but also in some of *Globigerinoides ruber* (white variety) which, in the studied area, are supposed to reflect upper thermocline and sea surface (mixed layer) conditions, respectively [*Fairbanks et al.*, 1982]. According to preliminary (oxidatively cleaned ICP-MS) downcore Mn/Ca data, five intervals were selected for this study, containing different concentrations of manganese, from the Late Holocene to Marine Isotopic Stage (MIS) 5 (Figure 3; Table 1).

[20] 1. Identification of contaminant phases: A first screening (Figure 2) of whole uncleaned *N. dutertrei* tests (3–5 individuals per sample) from the five previously selected intervals was analyzed by means of LA-ICP-MS facilities at the Research School of Earth Sciences (Australian National University).

[21] 2. Efficiency of cleaning protocols removing contaminant phases: Relatively large monospecific samples of *N. dutertrei* (about 50 specimens) were picked from the 315–355 μm size fraction in the five selected intervals (Table 1). Samples were then

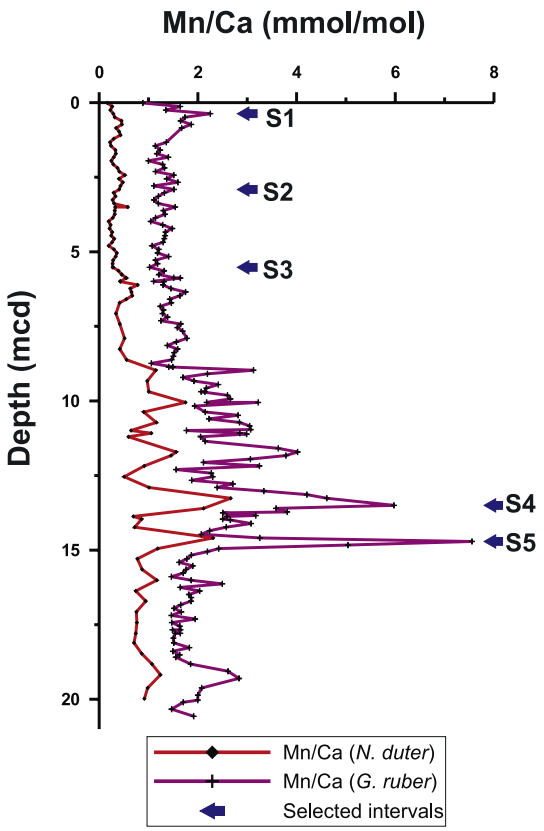

Figure 3. Late Pleistocene downcore Mn/Ca records from Site 1240 (expressed in mmol/mol). *G. ruber* (red line) and *N. dutertrei* (purple line) profiles are shown. Note the systematic offset between *G. ruber* and *N. dutertrei* values, the former having consistently higher Mn/Ca concentrations. Blue arrows point toward the selected intervals for this study (S1–S5).

crushed and well homogenized before split into two subsamples which were cleaned following two different cleaning protocols ("oxidative" cleaning and "reductive" cleaning protocols; Figure 2). Homogenization was particularly important to minimize any intrasample variability and provide comparable results between the two subsamples. After the cleaning of each subsample, individual fragments were picked and reserved for LA-ICP-MS analyses. The rest of the fragments were dissolved for bulk ICP-MS analyses.

[22] 3. Efficiency of the individual cleaning steps: Additionally, relatively large monospecific samples of *N. dutertrei* and *G. ruber* (about 50 specimens) were picked from the 315–355 μm size fraction in the five selected intervals (Table 1). As in the previous phase, samples were crushed and then well homogenized before split into two subsamples. After this, the two sets of subsamples were cleaned following the "reductive" cleaning protocol, but changing the order between the oxidative and reductive steps. The first batch of samples was cleaned following the sequence clay-oxidative-reductive-weak acid leaching, whereas in the second batch of samples, we followed the sequence clay-reductive-oxidative-weak acid leaching. In order to test the effectiveness of the different cleaning steps, we kept all liquid residues after every single cleaning step (i.e., clay removal, reductive phase, oxidative phase and weak acid leaching) and analyzed their element composition (after acidification) by ICP-MS. In these residues, we analyzed specifically Ca, Mg, Mn, Sr and Al. In parallel, we analyzed the cleaned foraminifera fragments and compared all results together.

[23] 4. Characterization of the contaminant phase: XRD analyses were carried out in sample SD-5, the one with highest manganese concentrations within the selected intervals. We picked about 20 mg of monospecific foraminifera *N. dutertrei* (∼700 individuals) from the 315–355 μm size fraction. Then, foraminifera were ground to powder in an agate mortar and spread over a monocrystalline silicate slide for analysis (see section 3.3 for analytical details).

[24] Additionally, *N. dutertrei* individuals from the same sample (SD-5) were cleaned following both the "reductive" and "oxidative" cleaning protocols. Cleaned single fragments were prepared (covered with a tiny layer of carbon) for SEM-EDX analyses providing semiquantitative element measurements from the foraminifera carbonate surfaces.

4. Results

4.1. Identification of Contaminant Phases

[25] We used LA-ICP-MS to monitor the manganese distribution within the foraminifera tests in a series of full uncleaned individuals of *N. dutertrei* from five selected intervals (SD 1–5). Depth profiles of Mg/Ca and Mn/Ca for different chambers are shown in Figure 4 together with the relationship between both elemental ratios (see figure caption for details). The most remarkable feature of the obtained results is the systematic appearance of an abrupt enrichment in Mn/Ca ratios accompanied also by an increase in Mg/Ca ratios always at the innermost part of the foraminifera shells. This Mn-Mg-enrichment occurs in all the samples analyzed and extends typically through 3–10 μm of thickness but with a wide range of variable absolute values. Consistently with our preliminary bulk data (Table 1, Figure 3)

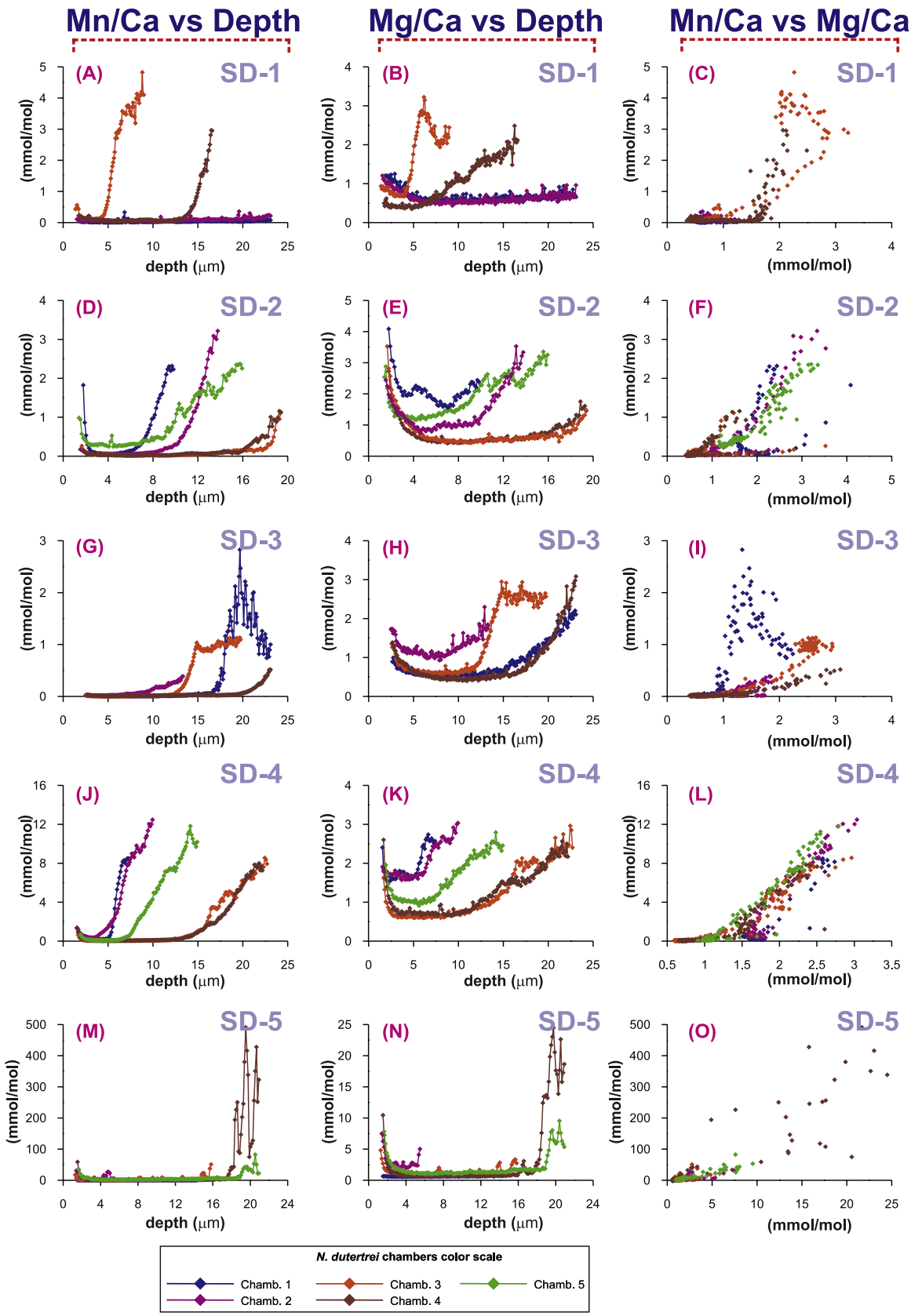
Mn/Ca vs Depth
Mg/Ca vs Depth
Mn/Ca vs Mg/Ca
(A) SD-1
(B) SD-1
(C) SD-1
(D) SD-2
(E) SD-2
(F) SD-2
(G) SD-3
(H) SD-3
(I) SD-3
(J) SD-4
(K) SD-4
(L) SD-4
(M) SD-5
(N) SD-5
(O) SD-5
(mmol/mol)
depth (μm)
N. dutertrei chambers color scale
Chamb. 1
Chamb. 2
Chamb. 3
Chamb. 4
Chamb. 5

Figure 4

samples SD 1–3 entail the lower values with enrichments typically of ~1–3 mmol/mol and 2–4 mmol/mol in Mg/Ca and Mn/Ca ratios, respectively (Figures 4a–4b, 4d–4e, and 4g–4h). These enrichments are far more extreme in the case of samples SD 4–5, with Mg/Ca and Mn/Ca ratios up to 25 mmol/mol and 400 mmol/mol, respectively (Figures 4j–4k and 4m–4n). The covariance between Mg and Mn is further illustrated in Figures 4c, 4f, 4i, 4l, and 4o. These results allow to establish clear differences between the "true" foraminiferal calcite, with relatively low Mn/Ca and Mg/Ca ratios (i.e., in the natural range of variability [*Lea*, 1999]), and an inner shell with extremely high Mn/Ca and Mg/Ca ratios.

4.2. Cleaning Protocols Removal Efficiency

[26] LA-ICP-MS depth compositional profiles from samples cleaned according to the "oxidative" cleaning protocol reveal the presence of inner shell Mg/Ca and Mn/Ca enrichments comparable to those previously observed in full uncleaned samples (Figures 5a–5b, 5d–5e, 5g–5h, 5j–5k, and 5m–5n). In general, Mg/Ca and Mn/Ca values at the inner part are 1–2 mmol/mol and 1–3 mmol/mol higher than in the rest of the shell, and only slightly lower than those measured in the uncleaned individuals (Figure 4). This ratio lowering, however, is not a systematic feature with some samples presenting slightly higher Mg/Ca and Mn/Ca ratios after the "oxidative" cleaning protocol. As for the uncleaned samples, Mg/Ca and Mn/Ca ratios present a strong linear relationship (Figures 5c, 5f, 5i, 5l, and 5o). It is worth to mention that the thickness of these enrichments (3–7 μm) is also comparable to that observed in the uncleaned samples. Bulk ICP-MS values, represented as horizontal (red) lines (Figure 5), provide Mg/Ca and Mn/Ca ratios which, in general, overestimate those ratios from "true" foraminiferal calcite.

[27] On the other hand, the results obtained for the same samples after the "reductive" cleaning protocol present a very different pattern (Figure 6). Even though the obtained elemental profiles still show some Mg/Ca and Mn/Ca enrichments at the innermost shell, their characteristics are very different from those appearing after the "oxidative" cleaning protocol. The thickness of the Mn-Mg-enrichments is substantially reduced, in most cases these layers are less than 2 μm thick. In addition, absolute values attained by the current inner shell enrichments are significantly lower by about 60% for Mg/Ca and about 99% for Mn/Ca (Figure 5). These results suggest that the reductive cleaning has efficiently removed most of the inner shell contaminant phases. These results are further supported by the bulk ICP-MS results (blue lines, Figure 6) which show Mg/Ca and Mn/Ca values which average the elemental ratios of the "true" foraminiferal calcite.

4.3. Efficiency of the Individual Cleaning Steps

[28] Results obtained from the bulk sample measurements after each of the cleaning approaches (Red-Ox and Ox-Red) demonstrate that there are no significant differences when exchanging the sequence order of the oxidative and reductive steps (Figure 7). In most cases, Mg/Ca ratios are indistinguishable within the error (%RSD variable between 2.7–6.2%) for both approaches (excepting sample SD-3). The same occurs in the case of Mn/Ca ratios, although in the case of samples with original high Mn/Ca ratios, the Reductive-Oxidative approach seems to be slightly more efficient that the Oxidative-Reductive one (see Tables 2a and 2b and Figure 7). Also noteworthy is the systematically higher Mn/Ca background level in *G. ruber* compared with *N. dutertrei*.

[29] The most interesting results from this experiment come from the elemental analysis of the residues of the different cleaning steps, which are presented in Figures 8 and 9 for *G. ruber* and *N. dutertrei*, respectively (see Tables 2a and 2b for the entire data set). Results are illustrated as 3-D plots, where concentrations of five analyzed elements (Ca, Mg, Mn, Sr and Al) are shown for the residues of each of the main cleaning steps (1st clay removal, 2nd clay removal, 3rd clay removal, reductive step, oxidative step and weak acid leach-

Figure 4. Laser ablation ICP-MS profiles from representative *N. dutertrei* individuals of five intervals (SD-1, SD-2, SD-3, SD-4, and SD-5; see Table 1 for details). Colored profiles were assigned to correlative chambers, ordered from the last (youngest) to the first chamber (eldest) in *N. dutertrei* individuals (i.e., 1 is the last formed chamber, and 5 is the first). Elemental ratios are expressed in mmol/mol, and depth profiles are expressed in μm. (a, d, g, j, and m) Mg/Ca versus depth profiles of different laser ablated chambers. (b, e, h, k, and n) Mn/Ca versus depth profiles of different laser ablated chambers. (c, f, i, l, and o) Mg/Ca versus Mn/Ca cross plots illustrating the linear relationship between both elements, particularly at the innermost parts of the foraminifera tests. Color arrangement is maintained, thereby making it possible to distinguish between different linear relationships for different chambers.

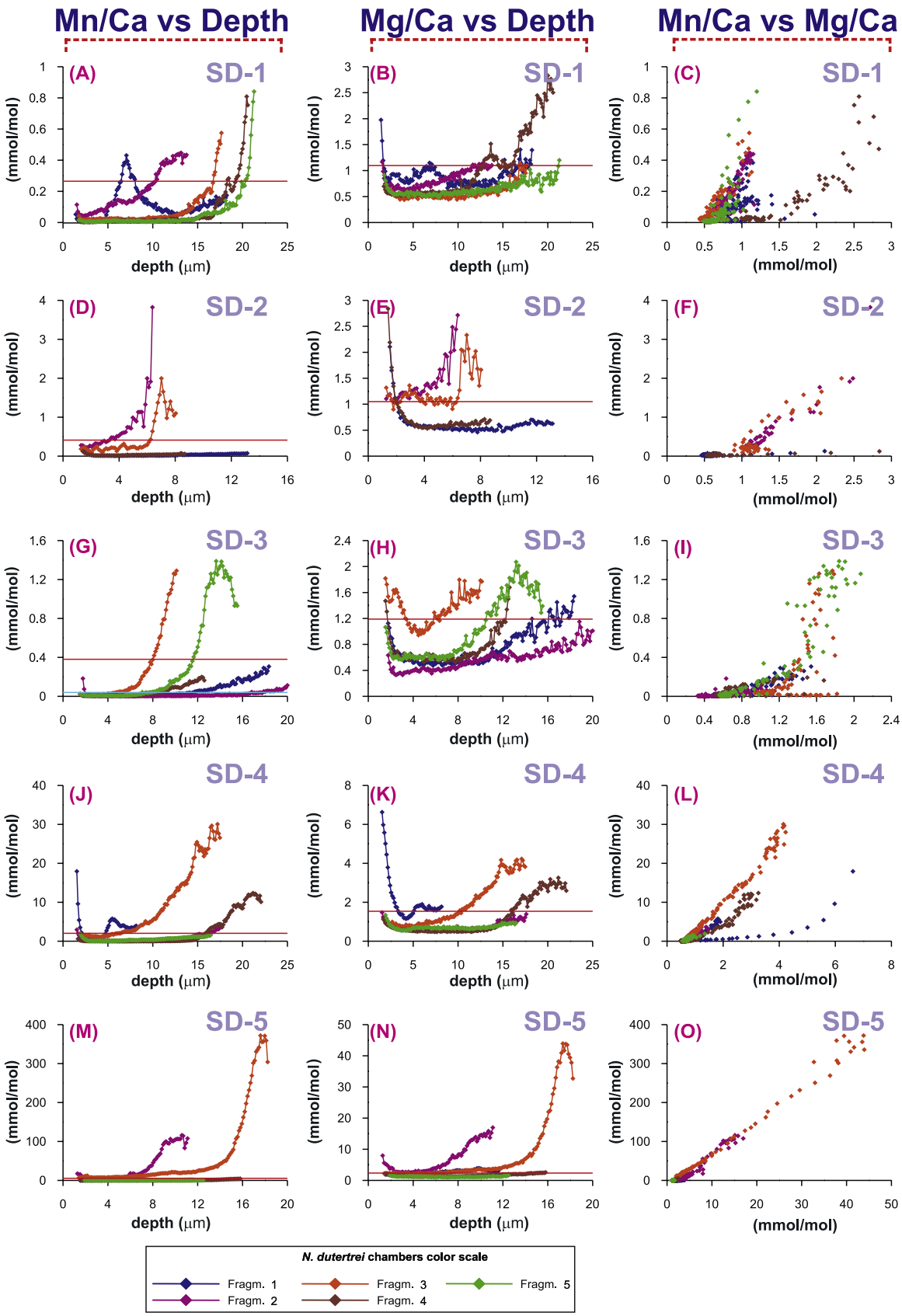
Mn/Ca vs Depth
Mg/Ca vs Depth
Mn/Ca vs Mg/Ca
(A) SD-1
(B) SD-1
(C) SD-1
(D) SD-2
(E) SD-2
(F) SD-2
(G) SD-3
(H) SD-3
(I) SD-3
(J) SD-4
(K) SD-4
(L) SD-4
(M) SD-5
(N) SD-5
(O) SD-5
(mmol/mol)
depth (μm)
N. dutertrei chambers color scale
Fragm. 1
Fragm. 2
Fragm. 3
Fragm. 4
Fragm. 5

Figure 5

ing-WAL). Two sets of plots per sample are shown, representing results from the Red-Ox and for the Ox-Red sequences. These graphs represent thus the "elemental fingerprint" of the residuals for the two different cleaning sequences. The study of these figures highlights the existence of two significantly different patterns or "elemental fingerprints" between the Red-Ox and Ox-Red sequences, which is consistent for both *G. ruber* (Figure 8) and *N. dutertrei* (Figure 9) samples.

[30] During the clay removal steps, particularly the first one, Mn and also Mg are removed in relatively low concentrations (Mn: 1–9 ppb; Mg: 1–7 ppb) with the exception of those samples with relatively high initial values of bulk Mn/Ca ratios (SR-5 in Figure 8 and SD-4, SD-5 in Figure 9), which show residual concentrations of 5–15 ppb and 5–10 ppb for Mn and Mg, respectively. Nevertheless, the removal of Mn is relatively low, considering the values of the bulk sample and only accounts for the 15–40% of the total Mn and 25–40% of the total Mg removed from the sample.

[31] Our results show that most of the Mn and Mg are removed during both the oxidative and reductive steps; however, large differences emerge when the order of these steps is exchanged. When the oxidative step is applied first, significant amounts of Mn (6–22 ppb for *G. ruber* and 5–16 ppb for *N. dutertrei*) and to less extent Mg (1–2 ppb for *G. ruber* and 1–3 ppb for *N. dutertrei*) is removed from the samples. On the other hand, Ca removal is almost insignificant (<0.3 ppb in all cases) as is the case of Sr and Al, (~1 ppb) (see Tables 2a and 2b for details). The subsequent reductive step appears to be the most effective step for removal of Mn (7.5–94.5 and 8–40 ppb for *G. ruber* and *N. dutertrei*, respectively) and Mg (7.8–22.7 and 6.6–17.3 ppb, respectively), but also for Sr (8–22.3 and 6–21 ppb, respectively), Ca (3–8.2 and 2.2–7.5 ppb, respectively) and even Al (1–2 and 2–4 ppb, respectively). However, when the reductive step is performed prior to the oxidative, the element concentrations of these reductive residuals are higher for Mn which range from (10–50 and 10–100 ppb for *G. ruber* and *N dutertrei*, respectively) (Figures 8 and 9), but similar for the remaining elements when we compare the previous reductive residuals (Mg: 5–20 ppb, Ca: 2–6 ppb, Sr: 5–20 ppb, Al: <5 ppb). In contrast, the oxidative step residuals in this Red-Ox sequence present extremely low Mn concentrations, always below 1 ppb. An interesting feature is that the sum of Mn concentrations removed during the Ox-Red sequence (oxidative step [Mn] + reductive step [Mn]) is equivalent to the amount of Mn removed during the single reductive step in the case of the Red-Ox sequence (Figures 8 and 9; Tables 2a and 2b).

[32] The last cleaning step, the weak acid leaching does not show major differences between the two different sequences. Mn concentrations in the residuals are not very significant, with values mostly below 1 ppb. This step seems to be more effective in the removal of Mg, Ca, Sr and also some Al but still in relatively low concentrations: Ca (0.5–1.7 ppb), Mg (2.1–4.9 ppb), Sr (1.3–4.8 ppb) and Al (2.4 ppb).

4.4. Characterization of the Contaminant Phase

[33] The final step of our experiment is to characterize the mineral composition and structure of the detected contaminant phase/s. There are still not many data available regarding the properties of the Mn phases that can be found associated with foraminiferal tests [*Boyle*, 1983]. With that intention, we have performed powder X-ray diffraction analyses (XRD) in a set of *N. dutertrei* individuals from the most manganese enriched interval (see details in section 3.3). Figure 10a shows the obtained diffractogram with major peak reflections coinciding closely with those expected from calcium carbonate. However, a closer view on the minor reflections reveals the presence of several mineral phases that are clearly different from the "pure" foraminiferal calcite (Figures 10b and 10c). These reflections match with those corresponding with the mineral kutnahorite, a mixed calcium-manganese-magnesium carbonate with general formula $Ca(Mn, Mg(CO_3)_2)$. In fact, there are three potential different classes of kutnahorite minerals

Figure 5. Laser ablation ICP-MS profiles from representative *N. dutertrei* shell fragments of five intervals (SD-1, SD-2, SD-3, SD-4, and SD-5; see Table 1 for details) cleaned according to the oxidative cleaning method. All the elemental ratios are expressed in mmol/mol, and depth profiles are expressed in μm. Note changes in scale from Figure 4. Horizontal lines correspond to bulk ICP-MS values measured in the same subsample splits after oxidative cleaning (red line). (a, d, g, j, and m) Mg/Ca depth profiles of different laser ablated shell fragments. (b, e, h, k, and n) Mn/Ca depth profiles of different laser ablated shell fragments. (c, f, i, l, and o) Mg/Ca versus Mn/Ca cross plots illustrating the still strong linear relationship between both elements, especially at the innermost parts of the foraminifera tests even after the oxidative cleaning process.

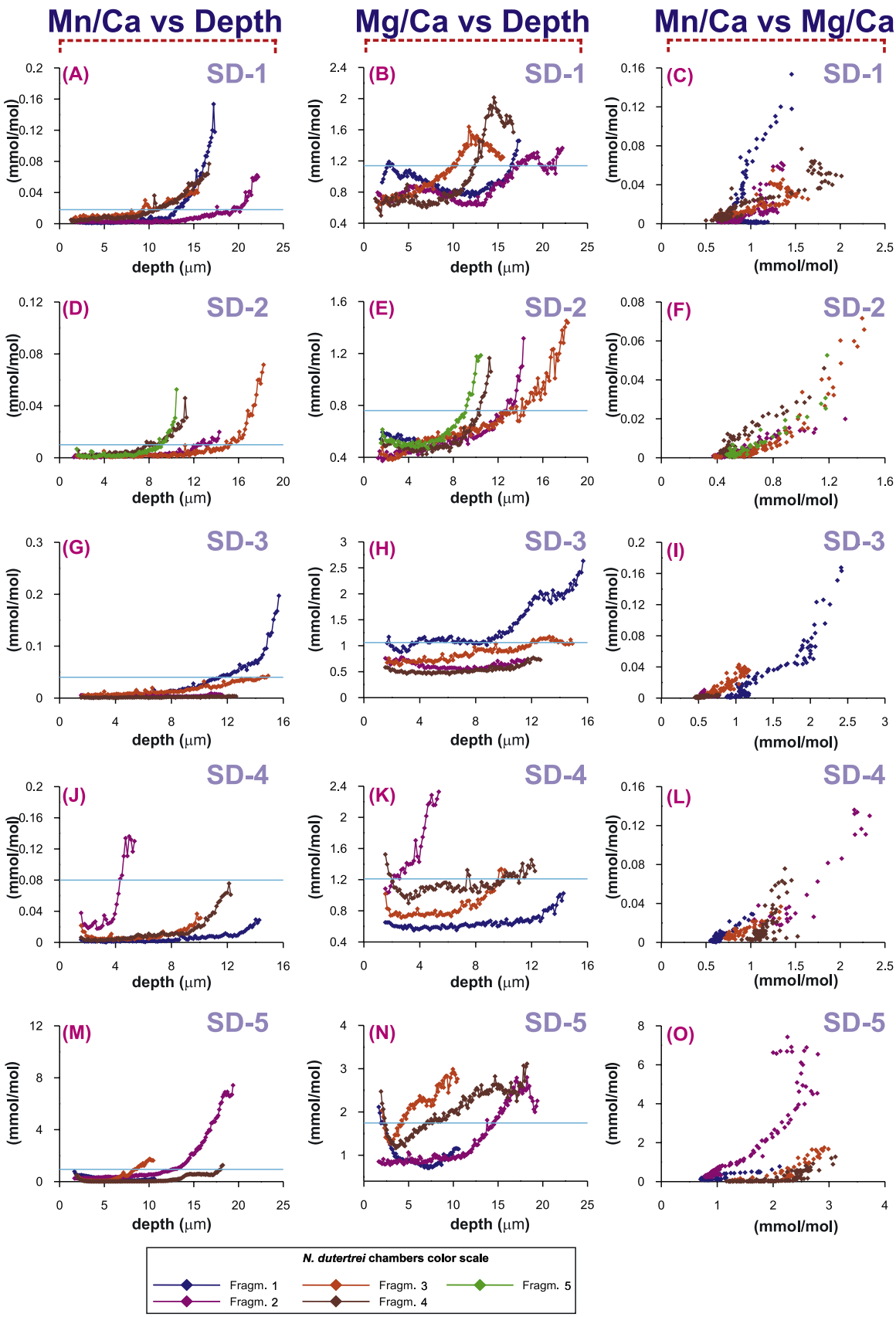
Mn/Ca vs Depth
Mg/Ca vs Depth
Mn/Ca vs Mg/Ca
(A) SD-1
(B) SD-1
(C) SD-1
(D) SD-2
(E) SD-2
(F) SD-2
(G) SD-3
(H) SD-3
(I) SD-3
(J) SD-4
(K) SD-4
(L) SD-4
(M) SD-5
(N) SD-5
(O) SD-5
(mmol/mol)
depth (μm)
N. dutertrei chambers color scale
Fragm. 1
Fragm. 2
Fragm. 3
Fragm. 4
Fragm. 5

Figure 6

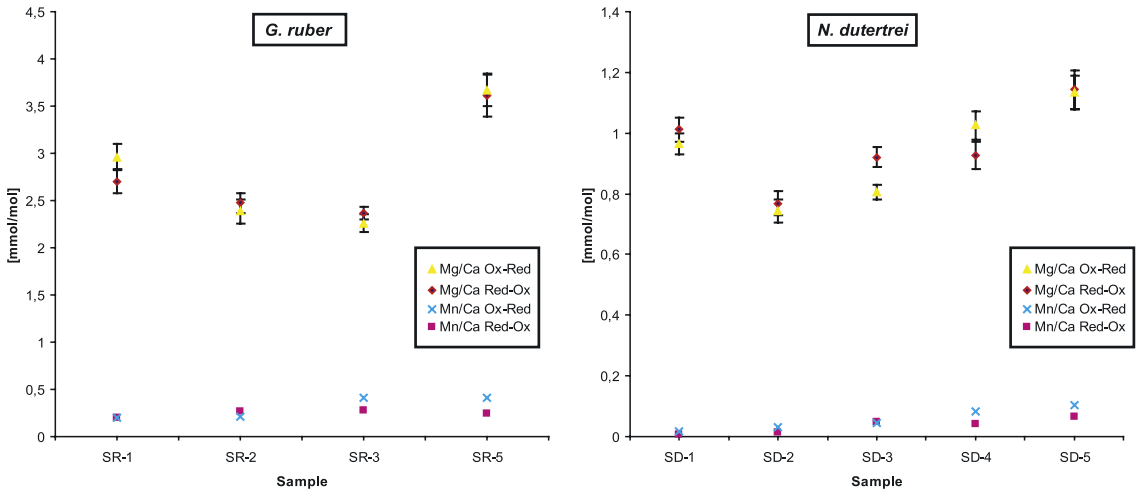

Figure 7. Simultaneous bulk ICP-MS measurements of Mg/Ca and Mn/Ca ratios in subsamples cleaned according to two different cleaning approaches of the full reductive cleaning protocol. *G. ruber* and *N. dutertrei* individuals from the same samples were cleaned, exchanging the order of the two most critical cleaning steps: reductive step and oxidative step. Results conclude that there is not a significant difference between Mg/Ca and Mn/Ca values produced according to the Red-Ox and Ox-Red approaches (with the only exception of sample SD-3). In the case of Mn-rich samples, the Red-Ox approach seems to be slightly more efficient than the Ox-Red approach. Error bars represent analytical %RSD variable between 2.7 and 6.2%.

that have been identified in this sample: "pure" kutnahorite ($CaMn(CO_3)_2$) (ICDD Powder Diffraction File, card 84-1290), magnesian kutnahorite ($Ca(Mn, Mg)(CO_3)_2$) (ICDD Powder Diffraction File, card 43-0695) and calcian kutnahorite ($Ca(Mn, Ca)(CO_3)_2$) (ICDD Powder Diffraction File, card 19-0234). The composition of natural manganese carbonates, including kutnahorites, is best represented by the ternary system $CaCO_3$-$MnCO_3$-$MgCO_3$ because they commonly display a continuum of compositions between calcite and rhodocrosite and contain 5–10 mol% $MgCO_3$ [*Peacor et al.*, 1987; *Mucci*, 2004]. However, it is worth to mention that this analytical technique does not allow distinguishing between single kutnahorite phases in the samples, but to point out the likely presence of multiple-kutnahorite phases (hereafter referred as "kutnahorite-like" phases).

[34] SEM imagery results for the same sample reveal the presence of a relatively thin carbonate layer at the inner surface of the fragment cleaned by the "oxidative" cleaning protocol (Figure 11a). EDX analyses show Mn and Mg spikes on this thin inner layer (Figure 11c). Consistently, the LA-ICP-MS elemental profile corresponding to that sample (Figure 11b) shows a very large Mn/Ca (up to 400 mmol/mol) and Mg (up to 50 mmol/mol) enrichments at the innermost part of the test. On the other hand, SEM images from the "Reductive" cleaned protocol fragments do not show this internal thin layer but the original porosity of the shell (Figure 11d). The absence of Mn and Mg spikes in the EDX scanning (Figure 11f) further support the removal of this thin contaminant layer by means of the "Reductive" cleaning protocol, which is in agreement with LA-ICP-MS results (Figure 11e).

5. Discussion

5.1. Characterization and Origin of the Mn-Mg Enrichments

[35] LA-ICP-MS results (Figure 4) clearly demonstrate the existence of Mn-Mg-rich phases attached to the inner foraminifera walls, which are unlikely to be the product of manganese oxides, since

Figure 6. Laser ablation ICP-MS profiles from representative *N. dutertrei* shell fragments of five intervals (SD-1, SD-2, SD-3, SD-4, and SD-5; see Table 1 for details) cleaned according to the full reductive cleaning method. All the elemental ratios are expressed in mmol/mol, and depth profiles are expressed in μm. Note changes in scale from Figures 4 and 5. Horizontal lines correspond to bulk ICP-MS values measured in the same subsample splits after full reductive cleaning (blue line). (a, d, g, j, and m) Mg/Ca depth profiles of different laser ablated shell fragments. (b, e, h, k, and n) Mn/Ca depth profiles of different laser ablated shell fragments. (c, f, i, l, and o) Mg/Ca versus Mn/Ca cross plots illustrating the weaker linear relationship between both elements after the reductive cleaning process.

Table 2a. Elements Concentrations (ppb) From *G. ruber* Samples Cleaned According to Two Different Approaches: Red-Ox and Ox-Red[a]

Sample Code	Cleaning Approach[b]	Ca(43), ppb	%rsd	Sr(88), ppb	%rsd	Mg(24), ppb	%rsd	Mn(55), ppb	%rsd	Al(27), ppb	%rsd
SR-1	Red-Ox	7.02	3.55	21.22	2.28	11.52	3.09	1.94	2.77	1.51	5.74
SR-2	Red-Ox	12.45	3.65	35.41	2.86	18.66	2.27	4.54	3.85	1.24	6.53
SR-3	Red-Ox	6.78	1.34	20.30	2.93	9.74	2.4	2.62	1.5	1.07	3.72
SR-5	Red-Ox	2.00	4.46	5.90	4.03	4.39	4.33	0.66	0.94	1.06	4.64
SR-1	Ox-Red	5.92	3.22	18.22	4.16	10.63	3.44	1.60	1.85	1.28	5.61
SR-2	Ox-Red	6.46	3.2	18.14	3.18	9.35	4.35	1.86	2.49	0.99	24.97
SR-3	Ox-Red	14.30	1.82	41.75	3.4	19.60	3.68	8.16	4.16	1.11	6
SR-5	Ox-Red	1.52	3.11	4.80	2.89	3.39	3.37	0.86	1.87	1.04	6.4
Clay Removal ruber: Residual Waste Element Concentration											
Clay-SR-1-1	none	0.56	5.15	1.83	3.32	4.01	4.2	5.98	0.48	0.58	10.62
Clay-SR-1-2	none	0.43	1.51	1.42	3.81	2.95	3.95	5.43	1.93	0.71	7.71
Clay-SR-1-3	none	0.41	2.59	1.29	3.67	2.11	4.33	3.54	2.99	0.63	6.21
Clay-SR-2-1	none	0.55	4.14	1.79	3.8	4.20	2.7	2.68	1.2	1.06	7.27
Clay-SR-2-2	none	0.60	2.39	1.76	2.79	2.93	3.44	3.73	2.36	0.76	5.31
Clay-SR-2-3	none	0.41	2.66	1.22	1.86	1.75	5.16	2.27	3.1	0.59	5.94
Clay-SR-3-1	none	0.53	3.1	1.73	3.98	2.97	3.9	3.81	4.15	0.70	6.63
Clay-SR-3-2	none	0.47	1.74	1.48	3.61	2.58	4.5	2.37	0.83	0.88	5.4
Clay-SR-3-3	none	0.53	4.77	1.54	4.01	3.32	4.61	1.74	2.45	0.76	23.97
Clay-SR-5-1	none	0.55	2.43	1.81	3.84	5.74	2.59	16.17	3.53	1.04	5
Clay-SR-5-2	none	0.99	2.91	2.97	2.68	4.55	5.98	17.93	2.11	0.69	6.07
Clay-SR-5-3	none	0.41	4.01	1.26	3.76	2.15	5.93	8.97	3.56	0.46	9.52
Reductive Cleaning											
Red-Clean-SR-1	Red-Ox	5.68	3.54	16.04	3.74	16.80	2.92	41.64	2.86	2.62	5.87
Red-Clean-SR-2	Red-Ox	4.88	3.26	13.28	4.17	14.09	3.36	33.57	3.39	2.17	5.26
Red-Clean-SR-3	Red-Ox	5.26	3.44	14.85	3.47	12.92	3.41	19.52	3.4	2.31	7.42
Red-Clean-SR-5	Red-Ox	4.71	2.07	13.53	3.06	15.71	3.23	61.73	2.45	2.39	5.97
Red-Clean-SR-1	Ox-Red	5.31	1.59	15.61	3.63	13.33	4.09	16.85	2.07	1.72	5.37
Red-Clean-SR-2	Ox-Red	7.52	3.35	21.05	3.28	17.33	1.3	16.15	2.5	2.55	2.93
Red-Clean-SR-3	Ox-Red	2.20	3.5	6.16	3.66	6.63	4.83	8.02	2.27	1.94	6.12
Red-Clean-SR-5	Ox-Red	6.44	2.3	18.87	4.24	17.02	3.56	39.21	2.31	1.93	5.11
Oxidative Cleaning											
Ox-Clean-SR-1	Red-Ox	0.13	6.16	1.30	3.19	1.77	4.25	0.36	1.08	0.68	5.13
Ox-Clean-SR-2	Red-Ox	0.14	3.76	1.16	2.13	3.93	1.85	0.77	3.31	1.11	3.8
Ox-Clean-SR-3	Red-Ox	0.14	4.4	1.14	3.69	1.82	3.13	0.40	4.55	1.01	6.25
Ox-Clean-SR-5	Red-Ox	0.12	3.63	1.07	3.46	1.84	3.21	0.12	4.4	0.76	5.52
Ox-Clean-SR-1	Ox-Red	0.09	3.97	0.83	2.82	0.89	5.28	15.83	2.53	0.65	7.54
Ox-Clean-SR-2	Ox-Red	0.14	2.58	1.00	2.26	0.87	5.12	16.30	1.86	0.65	3.84
Ox-Clean-SR-3	Ox-Red	0.06	14.17	1.22	4.82	1.83	3.84	5.91	2.31	0.94	5
Ox-Clean-SR-5	Ox-Red	0.09	4.6	0.83	4.29	1.59	6.71	22.09	2.04	1.10	5.36
Weak Acid Leach											
Weak-Ac-SR-1	Red-Ox	1.22	2.2	3.66	3.32	3.24	4.73	0.84	3.04	0.36	11.46
Weak-Ac-SR-2	Red-Ox	1.43	2.95	4.10	4.38	2.73	4.26	0.26	2.75	0.20	17.97
Weak-Ac-SR-3	Red-Ox	0.80	2.17	2.35	3.68	2.17	3.35	0.09	9.9	0.40	10.32
Weak-Ac-SR-5	Red-Ox	0.44	4.08	1.33	3.71	4.89	3.73	0.09	10.1	2.43	2.36
Weak-Ac-SR-1	Ox-Red	0.05	9.76	0.24	4.89	2.06	6.01	−0.03	28.77	0.08	48.36
Weak-Ac-SR-2	Ox-Red	0.24	4.14	0.68	5.34	4.29	5.12	0.10	6.95	13.48	4.29
Weak-Ac-SR-3	Ox-Red	0.26	3.48	0.78	4.14	10.19	4.12	0.31	3.7	5.61	7.52
Weak-Ac-SR-5	Ox-Red	0.09	9.1	0.28	4.56	3.14	4.5	0.02	29.13	0.28	20.32

[a] Residual wastes were also analyzed.
[b] All samples cleaned according to full reductive protocol.

Table 2b. Elements Concentrations (ppb) From *N. dutertrei* Samples Cleaned According to Two Different Approaches: Red-Ox and Ox-Red[a]

Sample Code	Cleaning Approach[b]	Ca(43), ppb	%rsd	Sr(88), ppb	%rsd	Mg(24), ppb	%rsd	Mn(55), ppb	%rsd	Al(27), ppb	%rsd
SD-1	Red-Ox	26.22	1.59	73.90	3.84	16.09	3.53	0.27	2.19	0.92	5.17
SD-2	Red-Ox	23.51	4.34	66.79	3.99	10.96	2.86	0.46	3.42	0.99	8.81
SD-3	Red-Ox	62.70	1.9	177.78	2.77	35.01	2.96	4.25	2.96	1.02	18.08
SD-4	Red-Ox	42.30	3.47	120.52	3.51	23.74	3.37	2.32	1.39	1.88	6.28
SD-5	Red-Ox	37.38	3.78	110.34	4.86	25.92	4.04	3.34	2.3	1.01	7.55
SD-1	Ox-Red	36.67	2.61	101.25	3.08	21.44	2.32	0.88	1.39	1.06	12.42
SD-2	Ox-Red	49.35	3.35	138.05	3.44	22.22	3.82	2.21	3.86	1.11	6.21
SD-3	Ox-Red	53.49	2.57	151.47	2.72	26.12	1.47	3.30	1.9	1.14	2.61
SD-4	Ox-Red	45.21	1.9	129.36	3.77	28.11	4	5.14	1.38	1.07	2.97
SD-5	Ox-Red	51.74	3.97	149.58	4.29	35.59	2.89	7.48	2.2	0.82	8.45
Clay Removal duter: Residual Waste Element Concentration											
Clay-SD-1-1	none	0.54	3.28	1.83	4.66	4.94	4.73	9.49	4.11	1.18	9.41
Clay-SD-1-2	none	0.48	4.29	1.37	2.55	1.83	3.82	3.11	1.28	0.70	8.91
Clay-SD-1-3	none	0.45	2.94	1.28	3.07	2.74	2.73	2.27	2.61	0.81	2.76
Clay-SD-2-1	none	0.54	3.04	2.25	3.4	5.80	2.63	5.42	2.76	1.62	4.45
Clay-SD-2-2	none	0.44	5.16	1.45	3.14	1.68	4.03	1.99	2.11	0.61	9.45
Clay-SD-2-3	none	0.50	3.28	1.39	3.77	1.33	6.19	1.34	3.05	0.61	11.45
Clay-SD-3-1	none	0.75	2.89	2.52	2.74	8.74	1.84	5.48	1.83	2.28	4.44
Clay-SD-3-2	none	0.48	1.93	1.40	2.96	2.10	2.25	2.55	4.12	0.88	7.89
Clay-SD-3-3	none	0.43	3.41	1.22	3.85	2.36	5.38	1.58	5.55	2.53	5.89
Clay-SD-4-1	none	0.55	3.8	1.93	2.69	9.51	1.91	21.77	2.94	2.18	14.28
Clay-SD-4-2	none	0.44	3.95	1.34	3.97	5.55	3.74	15.27	3.14	1.64	5.74
Clay-SD-4-3	none	0.44	3.72	1.25	3.87	3.60	4.01	11.91	2.28	1.30	12.41
Clay-SD-5-1	none	0.60	3.34	1.78	3.34	7.97	3.93	18.97	3.7	1.62	2.82
Clay-SD-5-2	none	0.44	5.08	1.31	5.45	3.66	5.7	9.97	2.12	0.80	6.74
Clay-SD-5-3	none	0.45	4.92	1.30	3.75	4.18	4.02	7.26	2.9	1.52	5.88
Reductive Cleaning											
Red-Clean-SD-1	Red-Ox	3.96	3.48	10.55	3.56	11.26	5.65	14.43	1.77	2.15	4.72
Red-Clean-SD-2	Red-Ox	3.37	3.45	9.32	1.87	6.37	3.35	9.19	0.64	2.02	4.91
Red-Clean-SD-3	Red-Ox	3.80	3.76	9.93	4.47	10.53	6	20.90	1.31	2.17	4.59
Red-Clean-SD-4	Red-Ox	6.26	5.02	16.71	3	15.23	2.52	135.69	3.46	2.14	4.4
Red-Clean-SD-5	Red-Ox	6.15	3.58	16.90	2.44	20.23	3.63	101.52	2.54	2.19	5.38
Red-Clean-SD-1	Ox-Red	3.04	1.69	8.09	5.16	7.78	3.85	7.50	2.29	4.34	4.03
Red-Clean-SD-2	Ox-Red	3.74	1.94	10.12	3.98	8.51	2.69	11.15	3	4.05	2.81
Red-Clean-SD-3	Ox-Red	4.41	3.14	11.77	3.07	7.86	3.46	9.67	2.46	2.05	4.78
Red-Clean-SD-4	Ox-Red	4.12	3.57	11.01	3.78	12.62	3.74	57.36	1.69	2.31	4.03
Red-Clean-SD-5	Ox-Red	8.20	1.34	22.37	1.9	22.71	2.41	94.53	1.38	2.53	2.91
Oxidative Cleaning											
Ox-Clean-SD-1	Red-Ox	0.11	8.37	1.13	4.17	3.13	3	0.07	7.95	1.19	4.29
Ox-Clean-SD-2	Red-Ox	0.10	6.43	0.91	3.12	1.52	4.32	0.15	6.17	0.91	8.34
Ox-Clean-SD-3	Red-Ox	0.19	5.11	1.38	4.65	2.22	4.35	0.75	3.22	0.89	7.75
Ox-Clean-SD-4	Red-Ox	0.12	4.4	1.04	4.18	2.23	3.82	0.77	2.95	1.32	4.2
Ox-Clean-SD-5	Red-Ox	0.12	4.72	0.23	2.2	2.49	2.01	0.03	7.4	0.68	33.3
Ox-Clean-SD-1	Ox-Red	0.09	3.72	1.02	4.91	2.07	5.65	8.02	2.43	1.03	6.15
Ox-Clean-SD-2	Ox-Red	0.10	11.04	1.11	4.01	2.45	4	11.09	2.65	0.84	17.24
Ox-Clean-SD-3	Ox-Red	0.07	8.87	0.97	3.34	1.06	6.79	4.97	1.17	1.63	8.71
Ox-Clean-SD-4	Ox-Red	0.28	2.74	1.48	3.62	1.04	5.32	12.98	2.8	0.82	4.55
Ox-Clean-SD-5	Ox-Red	0.11	9.08	0.89	4.47	2.57	5.19	16.09	1.64	1.08	5.48
Weak Acid Leach											
Weak-Ac-SD-1	Red-Ox	1.17	5	3.12	3.36	2.15	5.25	−0.02	16.95	0.49	7.93
Weak-Ac-SD-2	Red-Ox	1.05	3.69	2.98	4.79	2.71	6.09	0.02	51.99	0.76	8.33
Weak-Ac-SD-3	Red-Ox	1.35	4.2	3.73	3.07	2.54	4.12	0.14	6.14	0.31	12.24
Weak-Ac-SD-4	Red-Ox	1.72	5.07	4.77	5.18	2.47	4.46	0.12	7.67	0.37	13.89

Table 3. (continued)

Sample Code	Cleaning Approach[b]	Ca(43), ppb	%rsd	Sr(88), ppb	%rsd	Mg(24), ppb	%rsd	Mn(55), ppb	%rsd	Al(27), ppb	%rsd
Weak-Ac-SD-5	Red-Ox	1.34	4.52	3.78	4.74	2.34	5.84	0.24	3.65	0.29	11.76
Weak-Ac-SD-1	Ox-Red	0.21	2.22	0.64	2.75	3.04	2.11	0.03	11.68	0.99	2.96
Weak-Ac-SD-2	Ox-Red	0.21	6.27	0.66	4.68	1.06	7.82	−0.03	17.67	0.17	24.58
Weak-Ac-SD-3	Ox-Red	0.38	3.9	1.25	3.78	2.58	4.42	0.11	3.62	2.17	3.32
Weak-Ac-SD-4	Ox-Red	0.10	3.73	0.30	3.93	1.26	5.39	−0.04	11.86	0.55	7.47
Weak-Ac-SD-5	Ox-Red	0.44	3.86	1.30	3.97	3.15	5.96	0.16	9.95	2.17	6.91

[a] Residual wastes were also analyzed.
[b] All samples cleaned according to full reductive protocol.

MnO_x phases do not bear Mg in their crystal lattice. These results are consistent with XRD analysis which proves the occurrence of a "kutnahorite-like" carbonate mineral (Figure 10). It is important to note that rodochrosite ($MnCO_3$) has not been detected in our XRD analyses. However, the occurrence of "kutnahorite-like" minerals in our Panama Basin sediments indicates that the solubility of this mixed carbonate may be lower than that of the pure manganese carbonate phase [*Boyle*, 1983]. Mn/Mg ratios in "kutnahorite-like" carbonates cover a wide range of values, from ~7.3 [*Frondel and Bauer*, 1955] up to ~14 [*Peacor et al.*, 1987]. Our LA-ICP-MS results indicate that Mn/Mg ratios from the inner foraminiferal layers are about 8 (Figure 11b), and then consistent with the presence of a "kutnahorite-like" minerals. The empirical relationship of Mg/Ca versus Mn/Ca ratios determined for the contaminant phases in the ICP-MS analyzed samples is also in agreement with these conclusions. Given the Mn-contaminant phase is only fully removed with the "reductive" cleaning protocol, a further insight into the composition of this contaminant phase can be estimated by means of the difference in elemental ratios between results from the "oxidative" and the "reductive" cleaning protocols performed in the same samples (Figure 12). The obtained ratios (ΔMg/Ca and ΔMn/Ca) show a linear relationship with a slope of 0.11 (R = 0.8), meaning that for every unit reduction in Mn/Ca there is a 0.11 reduction in the Mg/Ca ratio. This value (i.e., 11%) is close to the 5–10% of Mg content that is considered to be included in kutnahorite-like carbonates [*Peacor et al.*, 1987; *Mucci*, 2004], further supporting our interpretations.

[36] The presence of "kutnahorite-like" phases in sediments from the Panama Basin as thin crusts within the sediment have been previously reported and linked with calcium carbonate rich sediments and coarser grain sizes [*Pedersen and Price*, 1982]. However, there is little data available regarding the properties of the Mn phases that occur associated with foraminiferal tests [*Boyle*, 1983]. Our results clearly document, for the first time, the presence of kutnahorite in foraminifera samples, and confirm the hypothesized formation of Mn-rich carbonate overgrowths in foraminifera tests by *Boyle* [1983]. Recently, it has been demonstrated that the abundance of calcite surfaces (i.e., reactive surfaces for nucleation of Mn-Mg bearing carbonates) is a critical factor controlling the appearance of "kutnahorite-like" minerals in marine sediments under suboxic/anoxic conditions [*Mucci*, 2004]. Our results are in agreement with these findings since Mn-Mg-rich carbonates are found at the inner surfaces of *N. dutertrei*, which present higher porosity and therefore more surface area for mineral nucleation. This suggests the most likely sequence of events leading to the formation of these Mn-Mg-rich carbonates is (1) a plentiful supply of manganese oxides from the water column (especially in high-productivity areas) reaches the sea floor sediments together with manganese coming from hydrothermal sources; (2) manganese oxides/hydroxides dissolve upon burial in the sediment as they enter reducing conditions (suboxic/anoxic sediments), and reduction of Mn(IV) to the more soluble Mn(II); and (3) Mn-Mg-rich carbonate is formed at the inner surface of foraminiferal tests due to the even more reductive microenvironment created inside the foraminiferal chambers [*Murray*, 1991] and also due to the reactive surfaces favoring carbonates nucleation [*Mucci*, 2004].

[37] Many different Mn-rich phases from different sources can coexist at the same time in the sedimentary record. For instance, high-productivity areas such as the Arabian Sea exhibit Mn-carbonates, Mn-oxides and also Mn associated with clays (aluminosilicates) and pyrites, all of which appearing simultaneously within the sedimentary record [*Schenau et al.*, 2002]. The analysis of our

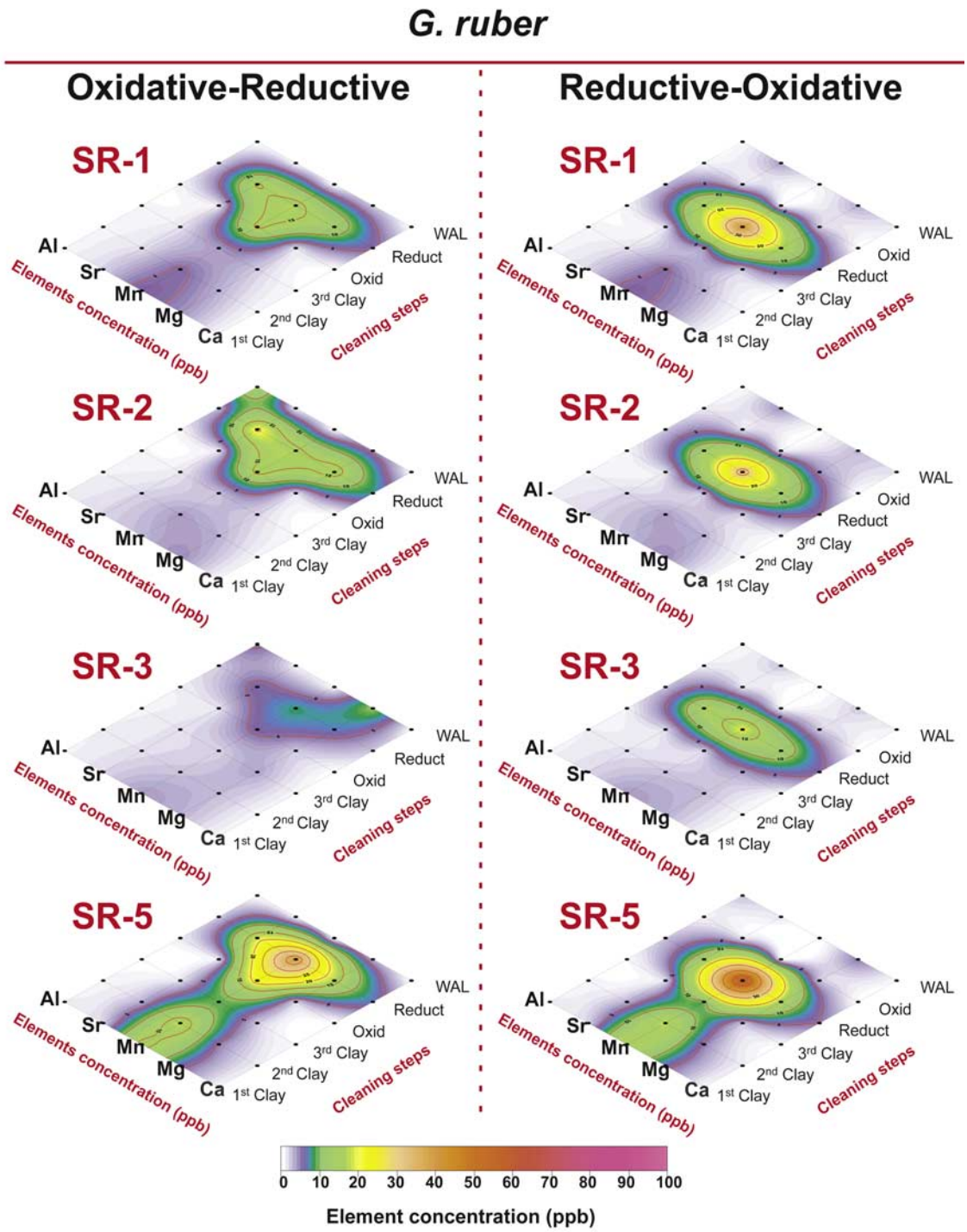

Figure 8. Single cleaning steps efficiency experiment in the case of two different cleaning approaches (Red-Ox and Ox-Red) of the "reductive" cleaning protocol when applied to four (SR-1–3 and SR-5) *G. ruber* samples. The plots shown represent the color concentration scale (in ppb) of different elements (Ca, Mg, Mn, Sr, and Al) as measured in the residual waste of every single cleaning step all through the cleaning protocol. Red lines illustrate iso-lines of concentration. Measurements were made by means of an ICP-MS device after acidifying the residuals (the entire data set produced is arranged in Table 2a). Cleaning protocol has been summarized into six main steps: three clay removal steps (1st Clay, 2nd Clay, and 3rd Clay; methanol rinses and final water rinse were excluded from the analyses), reductive step (Reduct), oxidative step (Oxid), and the final weak acid leaching (WAL). Thus each node in the figures represents the concentration of a certain element removed during a certain cleaning step. Note the similarity in the cleaning patterns or "elemental fingerprints" among samples cleaned following the same approach (i.e., Red-Ox or Ox-Red).

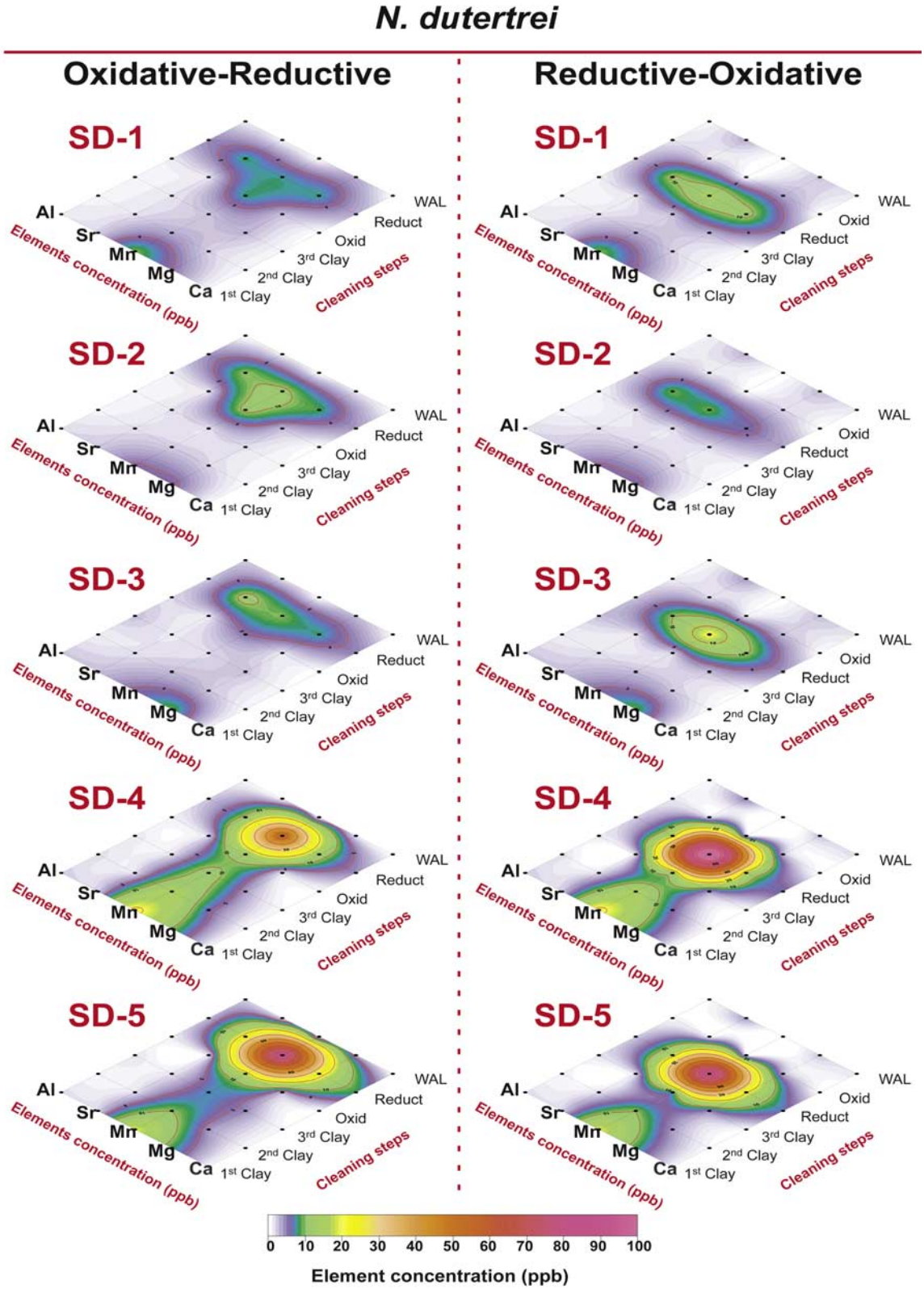
N. dutertrei
Oxidative-Reductive
Reductive-Oxidative
SD-1
SD-2
SD-3
SD-4
SD-5
Al
Sr
Mn
Mg
Ca
WAL
Reduct
Oxid
3rd Clay
2nd Clay
1st Clay
Cleaning steps
Elements concentration (ppb)
0 10 20 30 40 50 60 70 80 90 100
Element concentration (ppb)

Figure 9

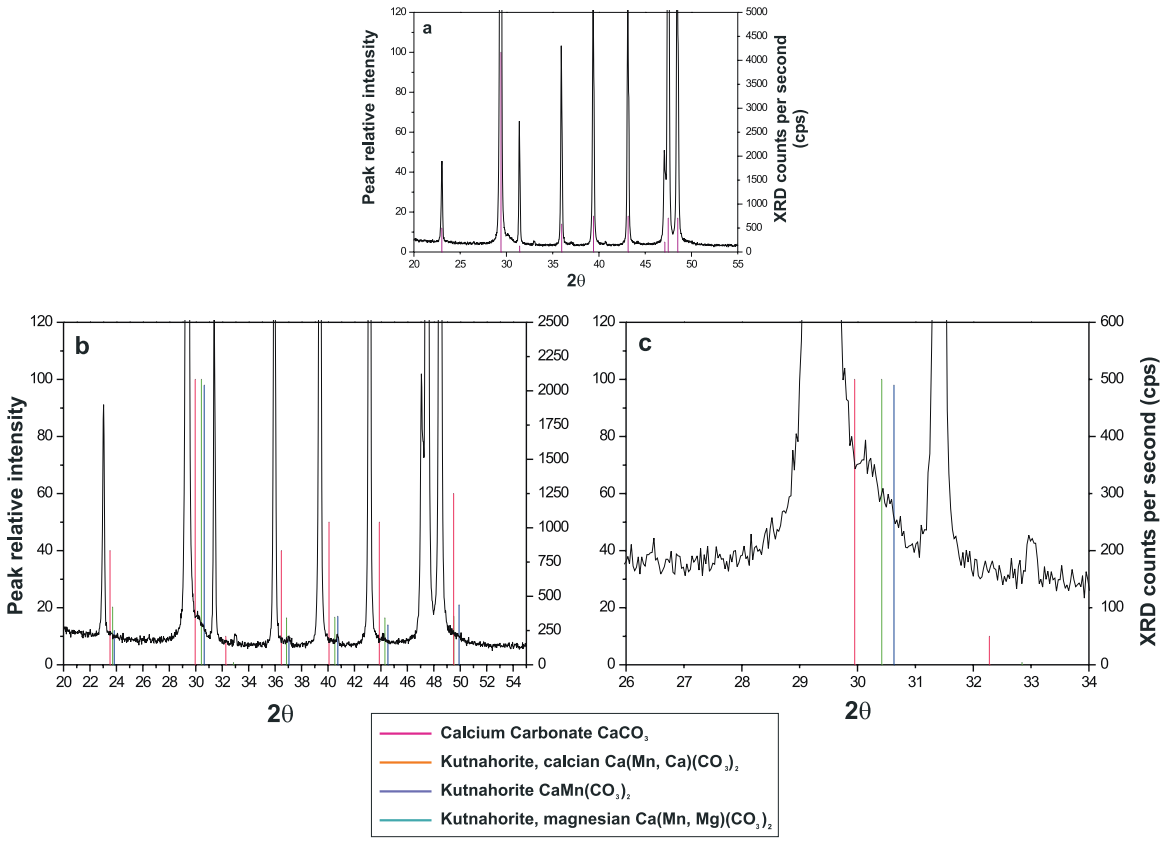

Figure 10. Powder X-ray diffractogram (XRD) obtained from about 20 mg of monospecific (*N. dutertrei*) foraminifera individuals in sample SD-5 (see Table 1 for details). Horizontal axis shows diffraction angles (2θ units), while vertical axis illustrates peak relative units and XRD counts per second (cps units). (a) X-ray diffractogram showing reflections matching perfectly with those corresponding to calcium carbonate ($CaCO_3$). (b) Zoom on the vertical scale presenting the theoretical lines of three kutnahorite-like minerals: kutnahorite ($CaMn(CO_3)_2$), kutnahorite calcian ($Ca(Mn, Ca)(CO_3)_2$), and kutnahorite magnesian ($Ca(Mn, Mg)(CO_3)_2$). (c) A detail on the kutnahorite-like reflections.

cleaning residuals (section 4.3) suggests that we have at least two different Mn phases coexisting in our samples (Figures 8 and 9). One phase which is only removed after the reductive step and we interpret to correspond mostly to ''kutnahorite-like'' carbonates and another phase which is removed either by the oxidative or the reductive steps but is not associated to anomalous high Mg values. We believe that this phase is likely related with organic matter as we will discuss more in detail in the next section. In addition to these two Mn-rich phases, the presence of Mn oxides in the foraminiferal tests cannot be completely ruled out.

5.2. Removal of Mn-Mg-Rich Contaminant Phases

[38] Considering the relatively high Mg values linked to the Mn-rich phases present in foraminiferal samples from the Panama Basin, the effectiveness

Figure 9. Single cleaning steps efficiency experiment in the case of two different cleaning approaches (Red-Ox and Ox-Red) of the full reductive cleaning protocol (''Cd cleaning'') when applied to five (SD-1–5) *N. dutertrei* samples. The plots shown represent the color concentration scale (in ppb) of different elements (Ca, Mg, Mn, Sr, and Al) as measured in the residual waste of every single cleaning step all through the cleaning protocol. Red lines illustrate isolines of concentration. Measurements were made by means of an ICP-MS device after acidifying the residuals (the entire data set produced is arranged in Table 2b). Cleaning protocol has been summarized into six main steps: three clay removal steps (1st Clay, 2nd Clay, and 3rd Clay; methanol rinses and final water rinse were excluded from the analyses), reductive step (Reduct), oxidative step (Oxid) and the final weak acid leaching (WAL). Thus each node on the figures represents the concentration of a certain element removed during a certain cleaning step. Note the similarity in the cleaning patterns or ''elemental fingerprints'' among samples cleaned following the same approach (i.e., Red-Ox or Ox-Red).

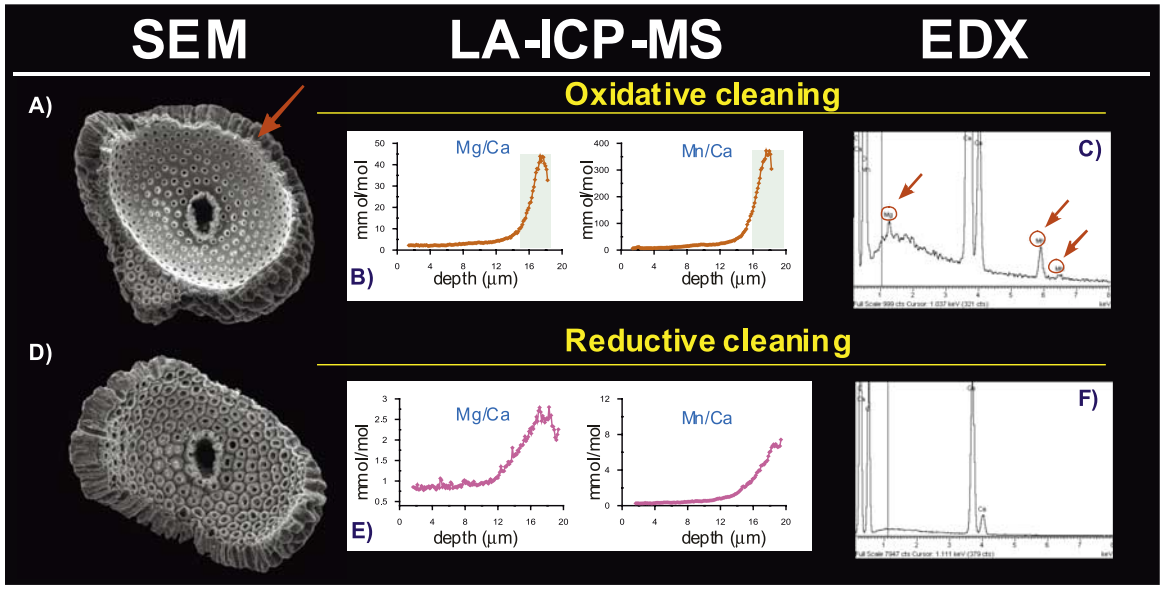

Figure 11. Compilation of results from Mn-rich sample SD-5. (a) SEM image of oxidatively cleaned ("Mg cleaning") *N. dutertrei* chamber fragment. Note the presence of a thin smooth layer at the innermost part of the test (red arrow), likely corresponding with kutnahorite-like contaminant phases. (b) LA-ICP-MS profiles (Mg/Ca and Mn/Ca) of the same shell fragment clearly indicating the presence of large enrichments in Mn/Ca and Mg/Ca at the innermost interval of the depth profile. Colored bands indicate the area of enrichments. (c) EDX elemental determination record at the inner surface of the same foraminifera fragment. Significant concentrations of Mn and Mg spiked during the analyses (red arrows). (d) SEM image of reductively cleaned ("Cd cleaning") *N. dutertrei* chamber fragment. There is no evidence of any layer or tiny patina at the innermost part of the test fragment. e) LA-ICP-MS profiles do not show large enrichments in Mg/Ca nor Mn/Ca ratios. (f) EDX analyses neither have detected any trace of Mn of Mn at the inner surface of the reductively cleaned shell fragment.

of the cleaning protocols becomes a critical issue in order to obtain accurate temperature reconstructions. The combination of both ICP-MS and LA-ICP-MS analyses has allowed precise monitoring of the effect that different cleaning protocols have on the foraminifera shell as well as to evaluate their consequences for paleoceanographic reconstructions. LA-ICP-MS depth profiles (Figures 5 and 6) demonstrate that these contaminant layers only disappear after the "reductive" cleaning protocol. A detailed inspection of the "elemental fingerprint" from the reductive residuals (Figures 8 and 9) further supports the effectiveness of the reductive step in the removal of Mn-Mg-rich carbonates and also probably Mn oxyhydroxides. SEM and EDX results also show that the "reductive" cleaning protocol is indeed able to dissolve Mn-Mg-rich inner shell layers (section 4.4; Figure 11).

[39] The question that now arises is why "kutnahorite-like" phases are removed by the reductive step. Selective dissolution of kutnahorite in front of calcite cannot be the reason since the solubility of this mixed carbonate phase should be less than that of the pure calcite [*Pedersen and Price*, 1982; *Boyle*, 1983; *Schulz and Zabel*, 2000]. Reductive cleaning is also

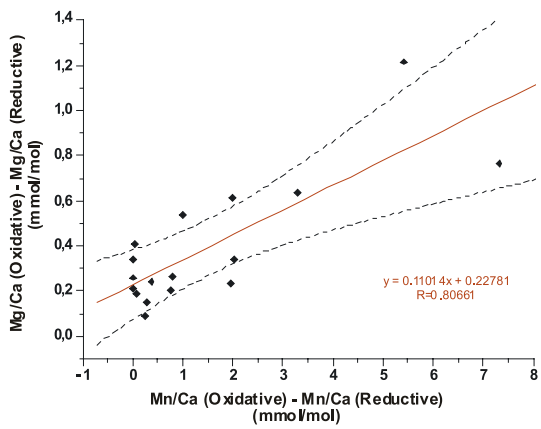

Figure 12. Linear relationship between the amounts of reduction (in mmol/mol) calculated by subtracting the Mn/Ca (oxidative) minus Mn/Ca (reductive) and Mg/Ca (oxidative) minus Mg/Ca (reductive) in a set of foraminiferal samples cleaned according to both methodologies. The 95% confidence intervals were also calculated (dashed lines). The slope obtained (0.11) closely matches the expected ratio of Mg in kutnahorite-like minerals (5–10%) [*Peacor et al.*, 1987; *Mucci*, 2004]. Correlation coefficient obtained is 0.80.

able to reduce Mn^{+4} to Mn^{+2} which is much more soluble and can be eliminated in the solution. Thus manganese oxides (MnO_x) are easily removed by this cleaning step. Reduction of Mn^{+4} could also account as the responsible mechanism for the removal of Mn associated to the organic matter, as has been illustrated to happen when the reductive step is done previously to the oxidative one (Figures 8 and 9). But, in any case it would explain the removal of the ''kutnahorite-like'' phases. The removal of kutnahorite may result from higher fragility of these very thin layers compared to the foraminifera wall (Figure 11). Another possibility could be the presence of MnO_x between the foraminifera shell and the carbonate layers, whose remobilization during the cleaning step promotes the exfoliation and dissolution of the kutnahorite layers. Regardless of the physical or chemical mechanism behind the kutnahorite removal, our results prove the need to proceed with the reductive step in order to ensure the adequate cleaning of the samples. Considering that Mn can be successfully removed with the reductive step prior to the oxidative one (Figures 8 and 9), it is tempting to argue that this oxidative step could be no longer necessary in the cleaning protocol. However, there are other elements, for example some traces of Mg, which is removed during the oxidative step of the cleaning, and that certainly needs to be eliminated in order to avoid potential contaminations in the measurements. The dearth of Mn, Ca and Sr in the analyzed residuals suggests that the Mg eliminated is rather linked to the oxidation of organic matter [*Hastings et al.*, 1992; *Rathburn and De Deckker*, 1997; *Rosenthal et al.*, 1997b] instead of dissolution of foraminiferal calcium carbonate. These results give further support to the consideration that the oxidative step is always necessary, whether it is carried after or before the reductive step does not seems to introduce a significant bias in the final results (Figure 7).

5.3. Implications of Mn-Mg-Rich Phases in Paleoceanographical Reconstructions

[40] The results presented here have shown the occurrence of biased Mg/Ca paleotemperatures estimations due to postdepositional formation of Mn-Mg-rich contaminant phases within foraminiferal tests. Inadequately cleaned samples can certainly account for significant past temperature overestimations if ''kutnahorite-like'' phases are formed upon early diagenesis processes. But the remaining question is: how important these biases are in terms of Mg/Ca ratios and therefore in temperature? Figure 13 shows Mg/Ca and Mn/Ca ratios differences between samples cleaned with the ''oxidative'' and ''reductive'' cleaning protocols of two different planktonic foraminifera species (*G. ruber* and *N. dutertrei*). A systematic decrease in Mg/Ca ratios takes place when the ''reductive'' cleaning protocol is applied, typically in the range of 7–36% (*N. dutertrei*) (Figure 13a) and 8–17% (*G. ruber*) (Figure 13b), and with the only exception of sample SD-5 (extremely rich in Mn), which has registered an Mg/Ca decrease of ~51%. When translated into temperature using the species specific [*Dekens et al.*, 2002] calibrations these reductions imply temperature decreases of 1 to 6.2°C (*N. dutertrei*) (Figure 13a) and 0.9 to 2.1°C (*G. ruber*) (Figure 13b), again with the exception of sample SD-5 (9°C reduction). Temperatures estimated after the ''oxidative'' cleaning protocol are unlikely to be ''realistic'' past temperatures. For example, sample SD-5 (Figure 13a) produced Mg/Ca temperature values of 30.6 ± 0.5°C (''oxidative'' cleaning protocol) and 21.5 ± 0.5°C (''reductive'' cleaning protocol). Oceanographic data show mean annual sea surface temperatures and upper thermoclyne temperatures at Site 1240 about 25°C and 20.5°C, respectively [*Conkright et al.*, 2001], which are much colder than the 30.6°C estimated for *N.* dutertrei individuals, an upper thermoclyne dweller [*Fairbanks et al.*, 1982]. Consequently, samples cleaned with the ''reductive'' cleaning protocol are actually recording more ''realistic'' temperatures, whereas samples cleaned by the ''oxidative'' protocol produce major temperature overestimations. Typically, Mn decreases after the ''reductive'' cleaning protocol in a range between 85–98.8% (*N. dutertrei*) (Figure 13c) and 73.2–96.8% (*G. ruber*) (Figure 13d). Higher Mn/Ca ratios from *G. ruber* samples indicate that this species is harder to be cleaned than *N. dutertrei*. We argue that the more porous texture of *G. ruber* could promote more readily the precipitation of ''kutnahorite-like'' minerals.

[41] It is not possible, however, to reject the possibility that some ''pure'' foraminiferal calcite may have been dissolved during the reductive cleaning step. It is known that partial dissolution on foraminiferal calcite lowers Mg/Ca ratios [*Brown and Elderfield*, 1996; *Rosenthal et al.*, 2000]. Results supported in Figures 8 and 9 point, to a certain extent, toward this possibility (releases of some Ca and Sr during the reductive step). Several workers have estimated different reductions in the Mg/Ca ratios: 10% in samples cleaned with reductive step versus samples cleaned without

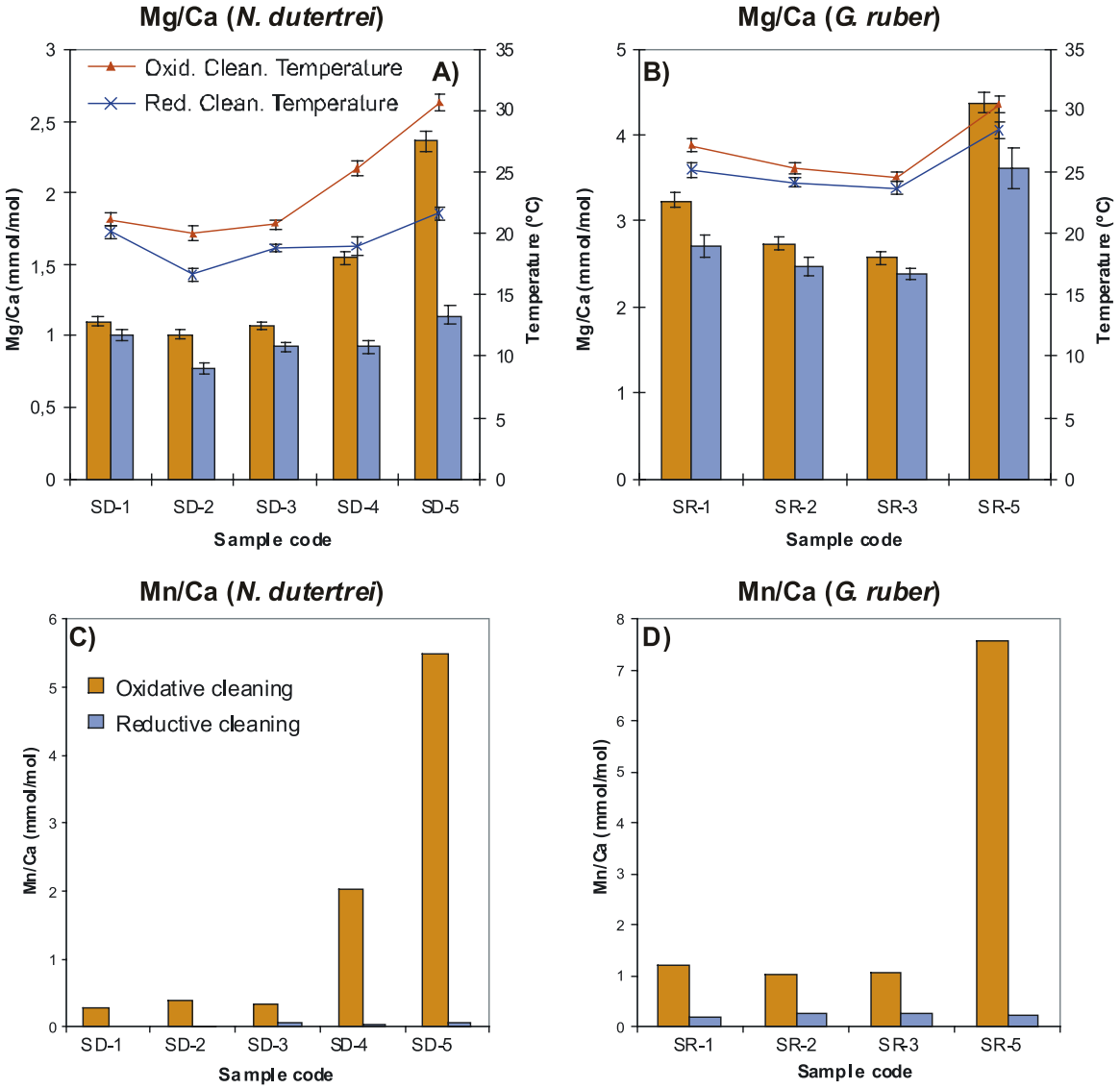

Figure 13. (a) Mg/Ca for five *N. dutertrei* samples cleaned according with both oxidative cleaning (orange bars) and reductive cleaning (blue bars). Equivalent temperature differences were calculated using the species specific calibration of *Dekens et al.* [2002]. (b) Mg/Ca differences between four *G. ruber* samples cleaned according to both oxidative cleaning (orange bars) and reductive cleaning (blue bars). Equivalent temperature differences were calculated using the species specific calibration of *Dekens et al.* [2002]. (c) Corresponding Mn/Ca differences between the five *N. dutertrei* samples cleaned following oxidative cleaning (orange bars) and reductive cleaning (blue bars). (d) Corresponding Mn/Ca differences between the four *G. ruber* samples cleaned according to both oxidative cleaning (orange bars) and reductive cleaning (blue bars).

a reductive step [*Martin and Lea*, 2002]; 10–15% between samples cleaned by the "reductive" and "oxidative" protocol [*Barker et al.*, 2003]. Likewise, *Rosenthal et al.* [2004] found a consistent bias of about 1°C between the "reductive" cleaning protocol and the "oxidative" cleaning protocol. However, these authors suggest that in practice, this problem is partly circumvented because workers tend to use regional Mg/Ca calibration performed with the same cleaning protocol to adjust their core top temperature estimates to the overlying observed hydrography [*Rosenthal et al.*, 2004]. Data from Site 1240 suggest that Mg/Ca reductions of up to 36% are rather beyond the effect of Mg/Ca decrease caused by partial solution of the foraminiferal shell during the reductive step. The dissolution of Mn-Mg-rich mineral phases must be responsible of a considerable part of this Mg/Ca reduction. Therefore we argue that the "reductive" cleaning protocol should be applied as a routine

whenever Mn-Mg-rich phases may be present in the foraminiferal samples. The partial dissolution of the "natural" foraminiferal shell that could be caused by this methodology is almost negligible (in terms of temperature) if local-cleaning specific Mg/Ca-Temperature calibrations are employed. Because of this methodology, a factor that introduces random Mg/Ca overestimations in the samples is being replaced by less significant systematic biases (toward lower Mg/Ca values) that can be simply corrected when translated into temperature estimations.

6. Conclusions

[42] LA-ICP-MS and SEM-EDX analyses demonstrate the presence of Mn-Mg-rich contaminant phases that typically occur as thin layers (3–10 μm) at the inner part of *N. dutertrei* shells from the Panama Basin. After mineralogical analyses based on XRD, we interpret this contaminant layer to be formed mainly by a Mn-rich carbonate kutnahorite, with the general formula $Ca(Mn, Mg)(CO_3)_2$). In fact, at least three different types of "kutnahorite-like" phases occur in the analyzed sample: "pure" kutnahorite, calcian kutnahorite and magnesian kutnahorite. This interpretation is further supported by the estimated percentages of Mg present in the contaminant phase (about 11% of Mg). But the existence of at least two different Mn phases coexisting in the samples is demonstrated by the analysis of cleaning residuals. One of these phases is only removed after the reductive step and we interpret this to mostly correspond to the "kutnahorite-like" carbonates whereas the other Mn-rich phase is removed with either the oxidative or reductive steps and we associate it to organic matter. Moreover, we cannot rule out Mn oxyhydroxides as an additional source of manganese in our Panama Basin samples.

[43] Inadequate cleaning samples can clearly result in significant overestimation of past seawater temperatures. For the Panama Basin samples analyzed in this study, Mg/Ca ratios are biased upward by typically 7–36% (*N. dutertrei*) and 8–17% (*G. ruber*). These biases correspond to significant temperature overestimates of 1.0–6.2°C (*N. dutertrei*) and 0.9–2.1°C (*G. ruber*). Paired LA-ICP-MS and ICP-MS measurements show that the "reductive" cleaning protocol can satisfactorily remove most of the Mn-Mg-rich phases from the samples and therefore eliminate the overestimation in the Mg/Ca ratios introduced by these diagenetic phases. However, we are unable to exclude the possibility that some partial dissolution of the "true" foraminiferal calcite may be also occurring during this process. Nonetheless, this latter effect can be partially circumvented by the application of regional, species specific calibrations that are constructed with samples having been subjected to the same cleaning protocols.

Acknowledgments

[44] L.P. and I.C. acknowledge a fellowship from the Comer Abrupt Climate Change Foundation (USA). Funding for this research was also provided by the Natural Environment Research Council through UK-ODP. C.P. also acknowledges support through a Ramón y Cajal contract from the Spanish Ministry of Education and Science during the last stages of this work. The manuscript was improved following constructive reviews from Peggy Delaney and an anonymous reviewer and helpful comments from the G^3 Associate Editor, Pamela Martin. Faviola Lacueva (IJA-CSIC) is thanked for her assistance and advice setting up the reductive step in the cleaning protocol. We greatly thank Nick J. Shackleton, Harry Elderfield, and Mervyn Greaves for comments and stimulating discussions. Roger Heady and Sally Stowe (Electron Microscope Unit at the Australian National University) are thanked for their assistance in obtaining SEM images. We also thank the Analytical Services Unit of the University of Barcelona, namely, Toni Padró, for his technical support with the ICP-MS analyses, Xavier Alcobé with the XRD, and Ramón Fontarnau for the support with SEM-EDX analyses. This research used samples provided by the ODP. The ODP is sponsored by the NSF and participating countries under management of Joint Oceanographic Institutions (JOI), Inc. E.C., S.E., and C.P. acknowledge the Australian Research Council for funding.

References

Aller, R. C. (1990), Bioturbation and manganese cycling in hemipelagic sediments, *Philos. Trans. R. Soc. London, Ser. A*, *331*, 51–68.

Baker, P. A., P. M. Stout, M. Kastner, and H. Elderfield (1991), Large-scale lateral advection of seawater through oceanic crust in the central equatorial Pacific, *Earth Planet. Sci. Lett.*, *105*, 522–533.

Barker, S., M. Greaves, and H. Elderfield (2003), A study of cleaning procedures used for foraminiferal Mg/Ca paleothermometry, *Geochem. Geophys. Geosyst.*, *4*(9), 8407, doi:10.1029/2003GC000559.

Boyle, E. A. (1981), Cadmium, zinc, copper, and barium in foraminifera tests, *Earth Planet. Sci. Lett.*, *53*, 11–35.

Boyle, E. A. (1983), Manganese carbonate overgrowths on foraminifera tests, *Geochim. Cosmochim. Acta*, *47*, 1815–1819.

Boyle, E. A. (1988), Cadmium: Chemical tracer of deep-water paleoceanography, *Paleoceanography*, *3*, 471–490.

Boyle, E. A., and L. D. Keigwin (1985), Comparison of Atlantic and Pacific paleochemical records for the last 215,000 years: Changes in deep ocean circulation and chemical inventories, *Earth Planet. Sci. Lett.*, *76*, 135–150.

Boyle, E. A., and Y. Rosenthal (1996), Chemical hydrography of the south Atlantic during the Last Glacial Maximum: Cd vs. $\delta^{13}C$, in *The South Atlantic: Present and Past Circula-*

tion, edited by G. Wefer et al., pp. 423–443, Springer, New York.

British Oceanographic Data Centre (2003), *Centenary Edition of the GEBCO Digital Atlas* [CD-ROM], Liverpool, UK.

Brown, S. J., and H. Elderfield (1996), Variations in Mg/Ca and Sr/Ca ratios of planktonic foraminifera caused by postdepositional dissolution: Evidence of shallow Mg-dependent dissolution, *Paleoceanography*, *11*, 543–551.

Cronblad, H. G., and B. A. Malmgren (1981), Climatically controlled variations of strontium and magnesium in Quaternary planktonic foraminifera, *Nature*, *291*, 61–64.

Dekens, P. S., D. W. Lea, D. K. Pak, and H. J. Spero (2002), Core top calibration of Mg/Ca in tropical foraminifera: Refining paleotemperature estimation, *Geochem. Geophys. Geosyst.*, *3*(4), 1022, doi:10.1029/2001GC000200.

Delaney, M. L., A. W. H. Bé, and E. A. Boyle (1985), Li, Sr, Mg and Na in foraminiferal calcite shells from laboratory culture, sediment traps and sediment cores, *Geochim. Cosmochim. Acta*, *49*, 1327–1341.

Eggins, S., P. De Deckker, and J. Marshall (2003), Mg/Ca variations in planktonic foraminifera tests: Implications for reconstructing palaeo-seawater temperature and habitat migration, *Earth Planet. Sci. Lett.*, *212*, 291–306.

Eggins, S. M., A. Sadekov, and P. De Deckker (2004), Modulation and daily banding of Mg/Ca in Orbulina universa tests by symbiont photosynthesis and respiration: A complication for seawater thermometry?, *Earth Planet. Sci. Lett.*, *225*, 411–419.

Elderfield, H., and G. Ganssen (2000), Past temperature and $\delta^{18}O$ of surface ocean waters inferred from foraminiferal Mg/Ca ratios, *Nature*, *405*, 442–445.

Fairbanks, R. G., M. Sverdlove, R. Free, P. H. Wiebe, and A. W. H. Bé (1982), Vertical distribution and isotopic fractionation of living planktonic foraminifera from the Panama Basin, *Nature*, *298*, 841–844.

Frondel, C., and L. H. Bauer (1955), Kutnahorite: A manganese dolomite, $CaMn(CO_3)_2$, *Am. Mineral.*, *40*, 748–760.

Hastings, D. W., S. Emerson, B. Nelson, A. Mix, and J. Erez (1992), Vanadium in planktonic foraminifera as a paleoceanographic tracer of sediment redox conditions, *Eos Trans. AGU*, *73*(43), Fall Meet. Suppl., F273.

Hastings, D. W., S. R. Emerson, J. Erez, and B. K. Nelson (1996), Vanadium in foraminiferal calcite: Evaluation of a method to determine paleo-seawater vanadium concentrations, *Geochem. Cosmochim. Acta*, *60*(19), 3701–3715.

Hastings, D. W., A. D. Russell, and S. R. Emerson (1998), Foraminiferal magnesium in *Globigerinoides sacculifer* as a paleotemperature proxy, *Paleoceanography*, *13*(2), 161–169.

Hathorne, E. C., O. Alard, R. H. James, and N. W. Rogers (2003), Determination of intratest variability of trace elements in foraminifera by laser ablation inductively coupled plasma-mass spectrometry, *Geochem. Geophys. Geosyst.*, *4*(12), 8408, doi:10.1029/2003GC000539.

Johnson, K. S., K. H. Coale, W. M. Berelson, and R. M. Gordon (1996), On the formation of the manganese maximum in the oxygen minimum, *Geochim. Cosmochim. Acta*, *60*(8), 1291–1299.

Lea, D. W. (1999), Trace elements in foraminiferal calcite, in *Modern Foraminifera*, edited by B. K. Sen Gupta, pp. 259–277, Springer, New York.

Lea, D. W., and E. A. Boyle (1991), Barium in planktonic foraminifera, *Geochim. Cosmochim. Acta*, *55*, 3321–3331.

Lea, D. W., and P. A. Martin (1996), A rapid mass spectrometric method for the simultaneous analysis of barium, cadmium and strontium in foraminifera shells, *Geochim. Cosmochim Acta*, *60*(16), 3143–3149.

Lea, D. W., T. A. Mashiotta, and H. J. Spero (1999), Controls on magnesium and strontium uptake in planktonic foraminifera determined by live culturing, *Geochim. Cosmochim. Acta*, *63*, 2369–2379.

Martin, P. A., and D. W. Lea (2002), A simple evaluation of cleaning procedures on fossil benthic foraminiferal Mg/Ca, *Geochem. Geophys. Geosyst.*, *3*(10), 8401, doi:10.1029/2001GC000280.

Moore, T. C., Jr., G. R. Heath, and R. O. Kowsmann (1973), Biogenic sediments of the Panama Basin, *J. Geol.*, *81*, 458–472.

Mucci, A. (2004), The behavior of mixed Ca-Mn carbonates in water and seawater: Controls of manganese concentrations in marine porewaters, *Aquat. Geochem.*, *10*, 139–169.

Murray, J. W. (1991), *Ecology and Paleoecology of Benthic Foraminifera*, 397 pp., John Wiley, Hoboken, N. J.

Nürnberg, D., J. Bijma, and C. Hemleben (1996), Assessing the reliability of magnesium in foraminiferal calcite as a proxy for water mass temperature, *Geochim. Cosmochim. Acta*, *60*, 803–814.

Peacor, D. R., E. J. Essene, and A. M. Gaines (1987), Petrologic and crystal-chemical implications of cation order-disorder in kutnahorite [CaMn (CO3)2], *Am. Mineral.*, *72*, 107–120.

Pedersen, T. F., and N. B. Price (1982), The geochemistry of manganese carbonate in Panama Basin sediments, *Geochim. Cosmochim. Acta*, *46*, 69–74.

Rathburn, A. E., and P. De Deckker (1997), Magnesium and strontium composition of Recent benthic foraminifera from the Coral Sea, Australia and Prydz Bay, Antarctica, *Mar. Micropaleontol.*, *32*, 231–248.

Reichart, G. J., F. Jorissen, P. Anschutz, and P. R. D. Mason (2003), Single foraminiferal test chemistry records the marine environment, *Geology*, *31*(4), 355–358.

Reimers, C. E. (1987), An *in situ* microprofiling instrument for measuring interfacial pore water gradients: Methods and oxygen profiles from the North Pacific Ocean, *Deep Sea Res., Part A*, *34*, 2019–2035.

Rosenthal, Y., E. A. Boyle, L. Labeyrie, and D. Oppo (1995), Glacial enrichments of authigenic Cd and U in Subantarctic sediments: A climatic control on the elements oceanic budget?, *Paleoceanography*, *10*, 395–413.

Rosenthal, Y., E. A. Boyle, and N. Slowey (1997a), Temperature control on the incorporation of magnesium, strontium, fluorine, and cadmium into benthic foraminiferal shells from Little Bahama Bank: Prospects for thermocline paleoceanography, *Geochim. Cosmochim. Acta*, *61*, 3633–3643.

Rosenthal, Y., E. A. Boyle, and L. Labeyrie (1997b), Last glacial paleochemistry and deep water circulation in the Southern Ocean: Evidence from foraminiferal cadmium, *Paleoceanography*, *12*, 778–787.

Rosenthal, Y., M. P. Field, and R. M. Sherrell (1999), Precise determination of element/calcium ratios in calcareous samples using sector field Inductively Coupled Plasma Mass Spectrometry, *Anal. Chem.*, *71*(15), 3248–3253.

Rosenthal, Y., G. P. Lohmann, K. C. Lohmann, and R. M. Sherrell (2000), Incorporation and preservation of Mg in *Globigerinoides sacculifer*: Implications for reconstructing the temperature and oxygen isotopic composition of seawater, *Paleoceanography*, *15*, 135–145.

Rosenthal, Y., et al. (2004), Interlaboratory comparison study of Mg/Ca and Sr/Ca measurements in planktonic foraminifera for paleoceanographic research, *Geochem. Geophys. Geosyst.*, *5*, Q04D09, doi:10.1029/2003GC000650.

Schenau, S. J., G. J. Reichart, and G. J. De Lange (2002), Oxygen minimum zone controlled Mn redistribution in Arabian Sea sediments during the late Quaternary, *Paleoceanography*, *17*(4), 1058, doi:10.1029/2000PA000621.

Schulz, H. D., and M. Zabel (Eds.) (2000), *Marine Geochemistry*, 1st ed., 455 pp., Springer, New York.

Wu, G., and C. Hillaire-Marcel (1995), Application of LP-ICP-MS to benthic foraminifers, *Geochim. Cosmochim. Acta*, *59*(2), 409–414.